Heat flow from the Southeast Indian Ridge flanks between 80°E and 140°E: Data review and analysis

L. Géli,[1] T. C. Lee,[2] J. R. Cochran,[3] J. Francheteau,[4] D. Abbott,[3] C. Labails,[1] and D. Appriou[1]

[1] We analyze available heat flow data from the flanks of the Southeast Indian Ridge adjacent to or within the Australian-Antarctic Discordance (AAD), an area with patchy sediment cover and highly fractured seafloor as dissected by ridge- and fracture-parallel faults. The data set includes 23 new data points collected along a 14-Ma old isochron and 19 existing measurements from the 20- to 24-Ma old crust. Most sites of measurements exhibit low heat flux (from 2 to 50 mW m^{-2}) with near-linear temperature-depth profiles except at a few sites, where recent bottom water temperature change may have caused nonlinearity toward the sediment surface. Because the igneous basement is expected to outcrop a short distance away from any measurement site, we hypothesize that horizontally channelized water circulation within the uppermost crust is the primary process for the widespread low heat flow values. The process may be further influenced by vertical fluid flow along numerous fault zones that crisscross the AAD seafloor. Systematic measurements along and across the fault zones of interest as well as seismic profiling for sediment distribution are required to confirm this possible, suspected effect.

Citation: Géli, L., T. C. Lee, J. R. Cochran, J. Francheteau, D. Abbott, C. Labails, and D. Appriou (2008), Heat flow from the Southeast Indian Ridge flanks between 80°E and 140°E: Data review and analysis, *J. Geophys. Res.*, *113*, B01101, doi:10.1029/2007JB005001.

1. Introduction

[2] Since the first attempt to measure temperature gradients in seafloor sediments [*Petterson*, 1949], heat flow data have provided information about the cooling history of lithospheric plates after their generation at spreading centers. Since it has been realized, during the early seventies [e.g., *Lister*, 1972], that hydrothermal circulation is a primary mechanism of heat transfer near mid-ocean ridge crests and off-ridge areas, numerous efforts have been made to assess advective heat loss through the oceanic crust, for example, by direct borehole measurement associated with ocean drilling and by inferences from rock and fluid geochemistry. A comprehensive collection of reviews on major advances in heat flow studies and the state-of-the-art knowledge can be found in the work by *Davis and Elderfield* [2004] such as the discoveries of hydrothermal circulation [*Sclater*, 2004] and geothermal evidence for continuing circulation in the crust older than 60 Ma [*Von Herzen*, 2004].

[3] Now that the mechanisms of heat transfer and water circulation are better understood, the question is whether or not the present knowledge opens the way to new experiments, specifically designed for testing geodynamic hypotheses or mapping thermal anomalies within the upper mantle in areas where significant variations in temperatures are expected. This study concerns the flanks of the Southeast Indian Ridge (SEIR), an oceanic domain where mantle thermal anomalies of ∼50°C to 70°C are expected between the Saint Paul/Amsterdam Islands and the Australian-Antarctic Discordance (AAD) "cold spot" [*Weissel and Hayes*, 1974] (Figures 1 and 2). Models describing the conductive cooling of oceanic lithospheric plates [e.g., *Davis and Lister*, 1974] suggest that the theoretical surface heat flow on young crust of age *t* is approximately

$$q = \frac{k(T_m - T_0)}{\sqrt{\pi \kappa t}} \qquad (1)$$

where T_m and T_0 are the mantle and surface temperatures, respectively, k and κ are the thermal conductivity and diffusivity of the crust and/or lithosphere, respectively. Using commonly accepted lithosphere values ($k \sim 3$ W K^{-1} m^{-1} and $\kappa \sim 10^{-6}$ m^2 s^{-1}), equation (1) suggests that an axial mantle temperature change in T_m of 50° to 70°C will result in a corresponding change in heat flow of 5 to 7 mW m^{-2} along an isochron of age $t = 10$ Ma. Such magnitude of estimated changes by conductive cooling is far below the

[1]Marine Geosciences Department, Ifremer, Plouzané, France.
[2]Department of Earth Sciences, University of California, Riverside, Riverside, California, USA.
[3]Lamont-Doherty Geological Observatory of Columbia University, Palisades, New York, USA.
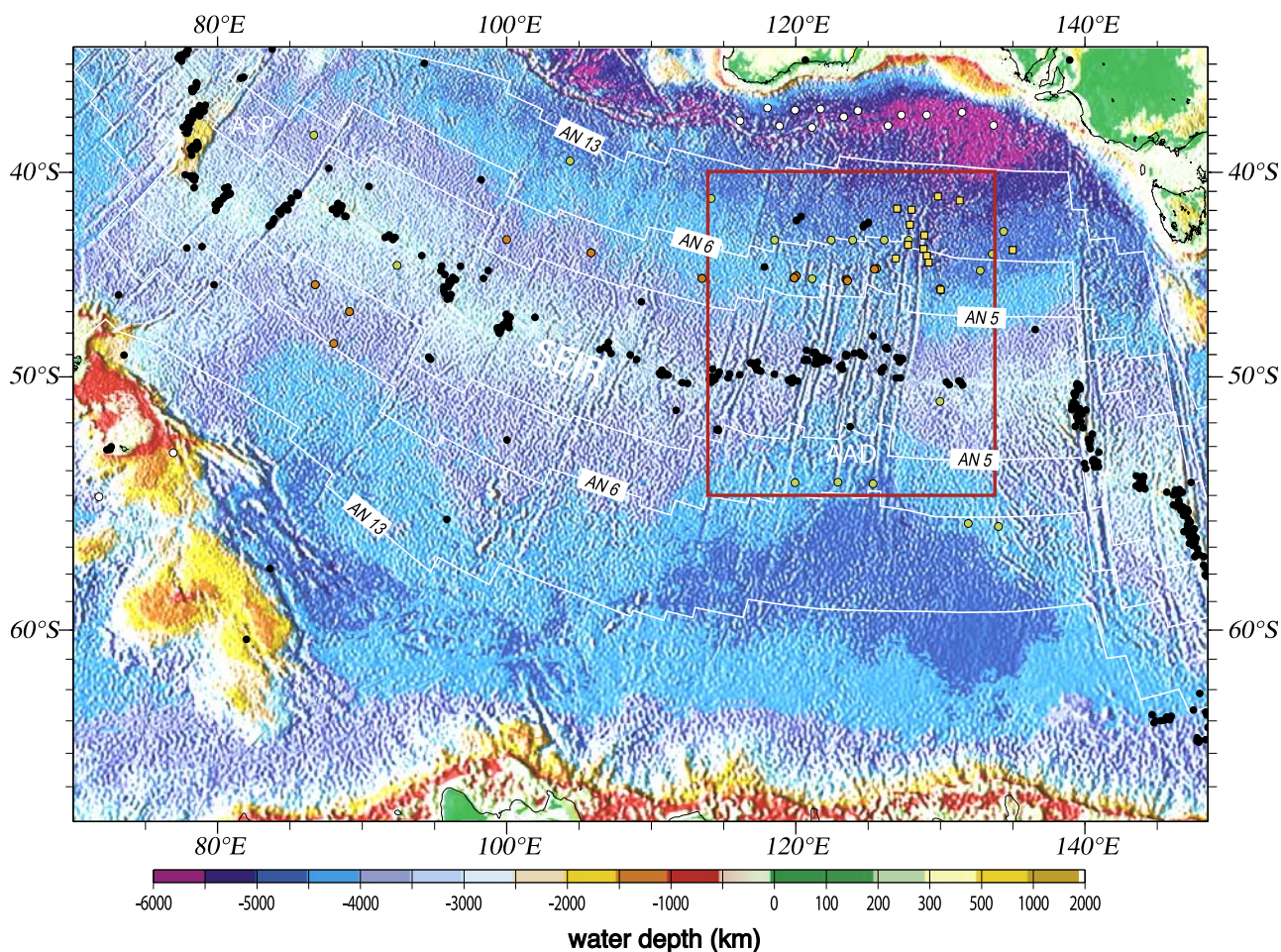[4]Institut Universitaire Européen de la Mer, Plouzané, France.

Figure 1. Predicted bathymetry in the study area [*Smith and Sandwell*, 1994]. Thin black lines indicate isochrons [after *Royer and Sandwell*, 1989]. The Southeast Indian Ridge, the Australian-Antarctic Discordance, and the Amsterdam and Saint Paul Islands are labeled as SEIR, AAD, and ASP, respectively. All stations with more than three temperature measurements within the sediment column are marked: orange dots for ages <42 Ma, white dots for ages >42 Ma are from the Lamont-Doherty Earth Observatory (LDEO) database, and green dots indicate *Marion Dufresne* heat flow sites locations. Yellow squares are ODP, Leg 187, drilling sites. White lines are magnetic isochrones labeled by anomalies An5, An6, An13, and An21). Black dots indicate earthquake locations after *Engdahl et al.* [1998]. The area enclosed by the red square is expanded in Figure 2.

anticipated variability due to environmental effects, such as hydrothermal circulation [e.g., *Louden and Wright*, 1989]. Here, we present new heat flow data and assess all data from the SEIR flanks in an attempt to decipher their implications, in context of all of these causes of variability.

2. Sediment Distribution in the AAD

[4] The distribution of sediment thickness can be glimpsed along a few regional seismic lines collected with the *Eltanin*, *Vema*, and *Conrad* research vessels in the mid-1960s and 1970s over the flanks of the SEIR (see examples in Figure 3). (Most seismic images are now available on http://www.marine-geo.org [*Carbotte et al.*, 2004].) Additional seismic data for the eastern boundary of the AAD were acquired during surveys over the northern flank prior to Ocean Drilling Program (ODP) Leg 187, using relatively light seismic equipment over the seafloor of age between

~14 and 28 Ma during the BMGR05 (1996) and SOJN05MV (1997) cruises. ODP Leg 187 also provides direct measurements of sediment thickness at drill sites (Figure 4). A seismic survey was not conducted during our Antaus cruise of R/V *Marion Dufresne* for heat flow measurements; however, we used a 3.5 kHz profiler to examine sediment covers when the ship was on heat flow stations.

[5] The AAD is a major passageway for Antarctic Deep Bottom Water (ADBW) to flow northward across the barrier at the South Indian Ridge [e.g., *Rodman and Gordon*, 1982; *Mantyla and Reid*, 1995; *Belkin and Gordon*, 1996]. This water forms in the Ross Sea and flows westward along the margin of Antarctica up to the Kerguelen Plateau, where it deviates to the north. Then, the ADBW follows the bathymetric contours on the southern flank of the SEIR to the AAD, and finally flow across the ridge to the north. Once passing the ridge, the water flows westward, following the
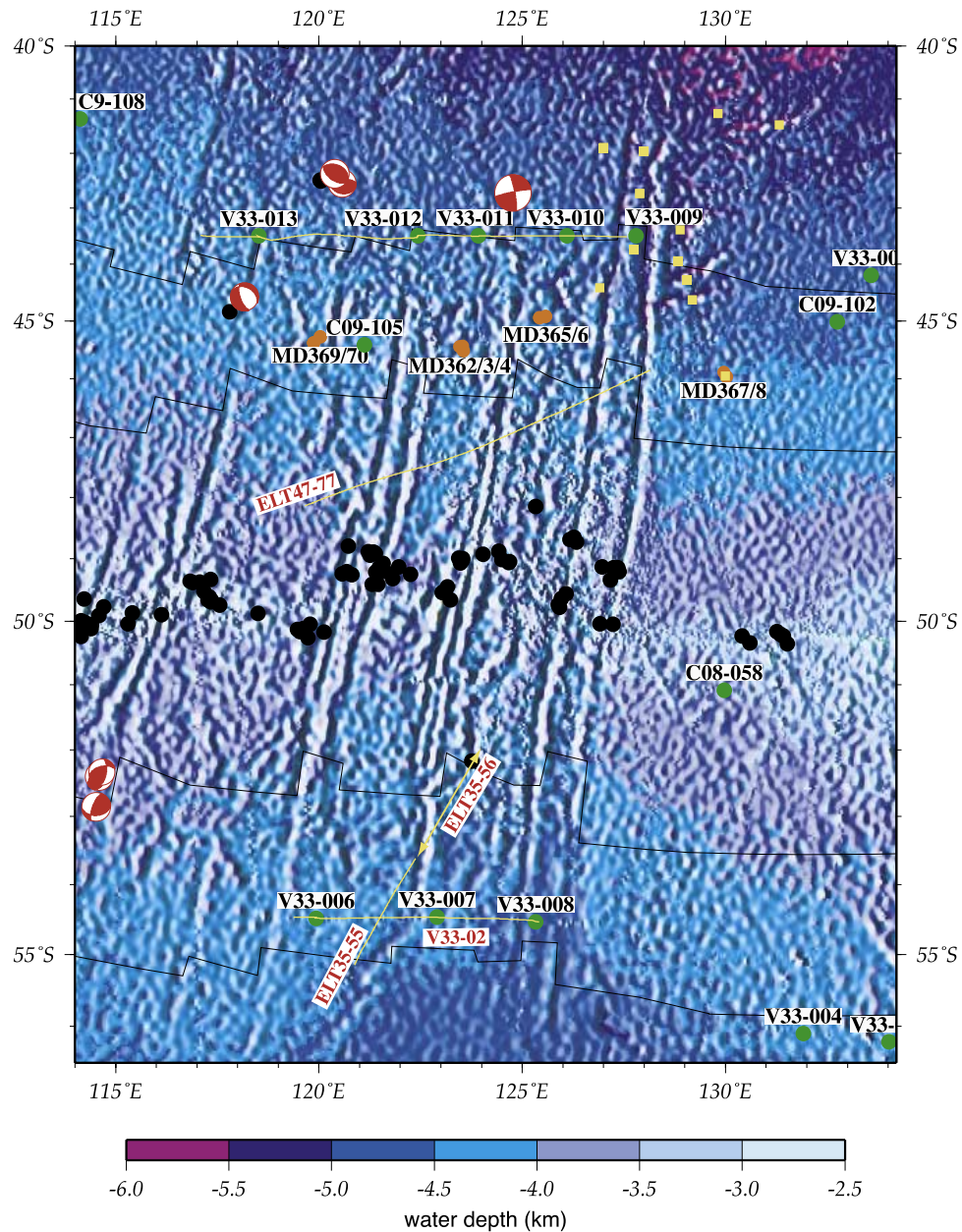
Figure 2. Bathymetry in the AAD area, as enlarged from Figure 1. Yellow lines stand for seismic tracks: ELT35, ELT47, and V33-02. Seismic sections ELT35-56 and V33-02 over the southern flank are depicted in Figure 3, and the other sections (ELT47-77 and ELT35-55) are available online at http://www.marine-geo.org/seislink/. Red and green dots indicate heat flow sites from the LDEO database and from *Marion Dufresne*, respectively, as flagged with their identification numbers. Yellow squares are ODP (Leg 187) drill sites [*Christie et al.*, 2004]. ODP data provide a direct measure of sediment thickness at drill sites and reveal that basalt has been weathered strongly by low-temperature hydrothermal circulation. Black dots represent earthquake epicenters after *Engdahl et al.* [1998]. Focal mechanism diagrams (from Harvard centroid moment tensor) are provided for intraplate earthquakes. Near 42.69°S and 124.69°E, a strike-slip, $M_w = 7.1$ earthquake occurred on 12 December 2001. Located on the 27-Ma old crust, this main shock was followed by numerous aftershocks. These earthquakes suggest that the tectonic fracturing is an ongoing process, which probably results in raising gross permeabilities of the oceanic crust.
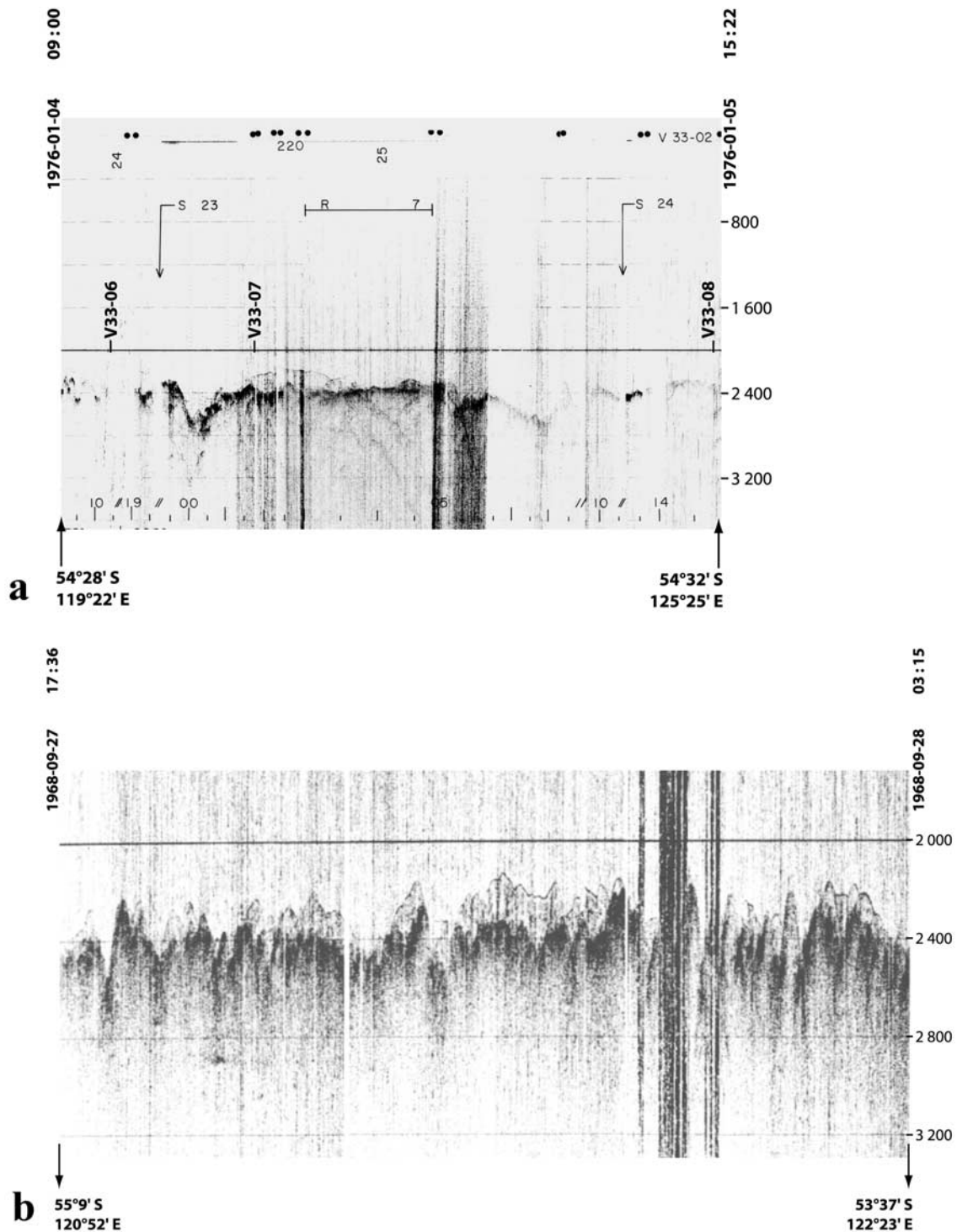
Figure 3. Selected seismic sections from the southern flank (see profile locations in Figure 2). (a) Line V33-02, with location of heat flow sites V33-06, V33-07, and V33-08. Note that the seismic acquisition was interrupted between sites V33-06 and V33-07, which are spaced ~200 km apart. (b) Section ELT035-55. The depth scale on the right is in fathoms (1 fathom = 1.83 m). Original seismic images are available on line at http://www.marine-geo.org/seislink.
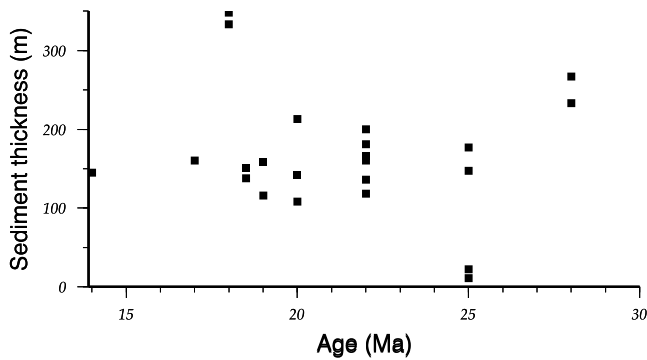
Figure 4. In situ sediment thickness directly measured at ODP187 drill sites versus crustal age (site locations are marked by yellow squares in Figures 1 and 2).

bathymetric contours on the northern flank of the ridge. Along the flow path, the water scours the seafloor sediments and redeposit the sediment load as contourites [*Dezileau et al.*, 2000]. Such scourings explain the depletion of sediment cover within the depressions of the ridge flanks with ages up to 20 to 25 Ma.

[6] Seismic lines ELT35 and V3302, which cross the north-south trending fracture zones on the 22-Ma old seafloor (Figure 4), provide some indications on the sediment distribution in the southern flank of the AAD. Along both lines, the sediments appear to drape over topographic highs. The sediments are siliceous oozes that are deposited in the valleys and swept away by the scouring bottom currents, both at the local and regional scales. This interpretation is supported by the fact that it is easier to core at topographic highs in the AAD area than in the valleys, as evidenced by frequent bending of corer upon penetration into the consolidated valley sediments (J.-L. Turon, personal communication, 2000).

3. Review of the Existing Data (30°–60°S; 70°–140°E)

[7] The database from the Lamont-Doherty Earth Observatory (LDEO) includes temperature measurements, estimates of geothermal gradients, sediment conductivity, and heat flux values, as well as information on data quality and errors. Other workers kindly provided additional and original data (which do not include error estimates or individual probe temperatures): K. Louden from Dalhousie University [*Louden and Wright*, 1989], C. Stein from Northwestern University [e.g., *Stein and Stein*, 1992, 1994], and A. Goncharov from Geoscience Australia. The latter provided a compilation from Australia that was originally reported by the Australian Geodynamics Center [*Somerville et al.*, 1994]. The full database used in this paper is provided in the auxiliary material.[1]

[8] The SEIR flanks, together with the Pacific-Antarctic Ridge flanks, appear to be one of the least covered regions of the world ocean in heat flow measurements. In our study area (30°–60°S; 70°–140°E), only a total of 111 data points

were collected from this area of 16 millions square kilometers, mainly during the mid-1960s and early 1970s. Most results have been published [*Von Herzen and Langseth*, 1966; *Langseth and Taylor*, 1967; *Hyndmann et al.*, 1974; *Anderson et al.*, 1977, 1979]. See also the review of heat flow measurements at drill sites by *Pribnow et al.* [2000].

[9] About 70% of those data were measured with the Ewing-type probes and the rest were acquired either with the Bullard-type probes or in boreholes. In a Ewing-type probe, temperature sensors are attached with outriggers onto a 6- to 15-m-long coring pipe. This allows retrieval of cores for conductivity measurements and other analyses. In contrast, no core can be taken with the Bullard-type probe, which consists of a 2-m-long tube, embedded with two or three thermal sensors (recent probes contain more sensors). Here, we exclude data sets that were based on only two sensor probes because of the inherit inability to assess vertical variability in geothermal gradient; we retain the data at 40 stations with at least three temperature measurements in the sediments. Among the 40 stations, 21 (identified as white dots in Figure 1) were located near the borders of the oceanic basins (mostly near the Southern Australia margin and near the Broken Ridge or near the Kerguelen Plateau margin), on crust older than about 55 Ma. The remaining 19 (green dots in Figure 1) were collected on crust younger than 31 Ma, hence poorly sedimented [e.g., *Goodell et al.*, 1973; *Hayes*, 1991]. The data distribution with respect to the underlying crustal age is not uniform: 17 out of the 19 measurements were from the 15- to 31-Ma old crust on the ridge flanks, and 2 were over the crust of less than 2 Ma old (Figures 1 and 2). These measurements resided in rough terrain [e.g., *Anderson et al.*, 1977], which, according to the classification by *Sclater et al.* [1976], falls into category D ("sediment ponded between or next to an obvious outcropping basement high") or at best, category C ("rough topography with a thin or variable sediment cover"). All measured heat flows (q_m) are lower than the theoretical value, q_c, prescribed by conductive lithospheric cooling models (based on equation (1)). In addition, most temperature profiles from the ridge flanks are fairly linear, except three at V33-003, V33-006, and C9-102 (Figure 5). If we exclude the two measurements (C8-048 and C8-058) over the very young crust (1.5 to 1.6 Ma old) and the three measurements displaying nonlinear geotherms (V33-003, V33-006, C9-102), the ratios of q_m/q_c range between about 35 and 55% (Figure 6).

4. New Data From R/V *Marion Dufresne*
4.1. Site Overview

[10] R/V *Marion Dufresne* is a 130 m long, multipurpose vessel, equipped with an array of bathymetry and imagery systems and with facilities for taking up to 65-m-long cores for investigation of sediments such as paleoclimatic records. During the 2000 Antaus cruise, we took the opportunity to collect high-quality thermal measurements at 22 stations (out of 25 attempts) and 14 gravity cores from the flanks of the Southeast Indian Ridge. Additionally, during the 2002 Carhot-Swift cruise, thermal measurements were made at three stations along with two gravity cores from the southern flank of the Southeast Indian Ridge. These 25 measurements were made at 11 sites (Table 1): 1 near 130°E (east of

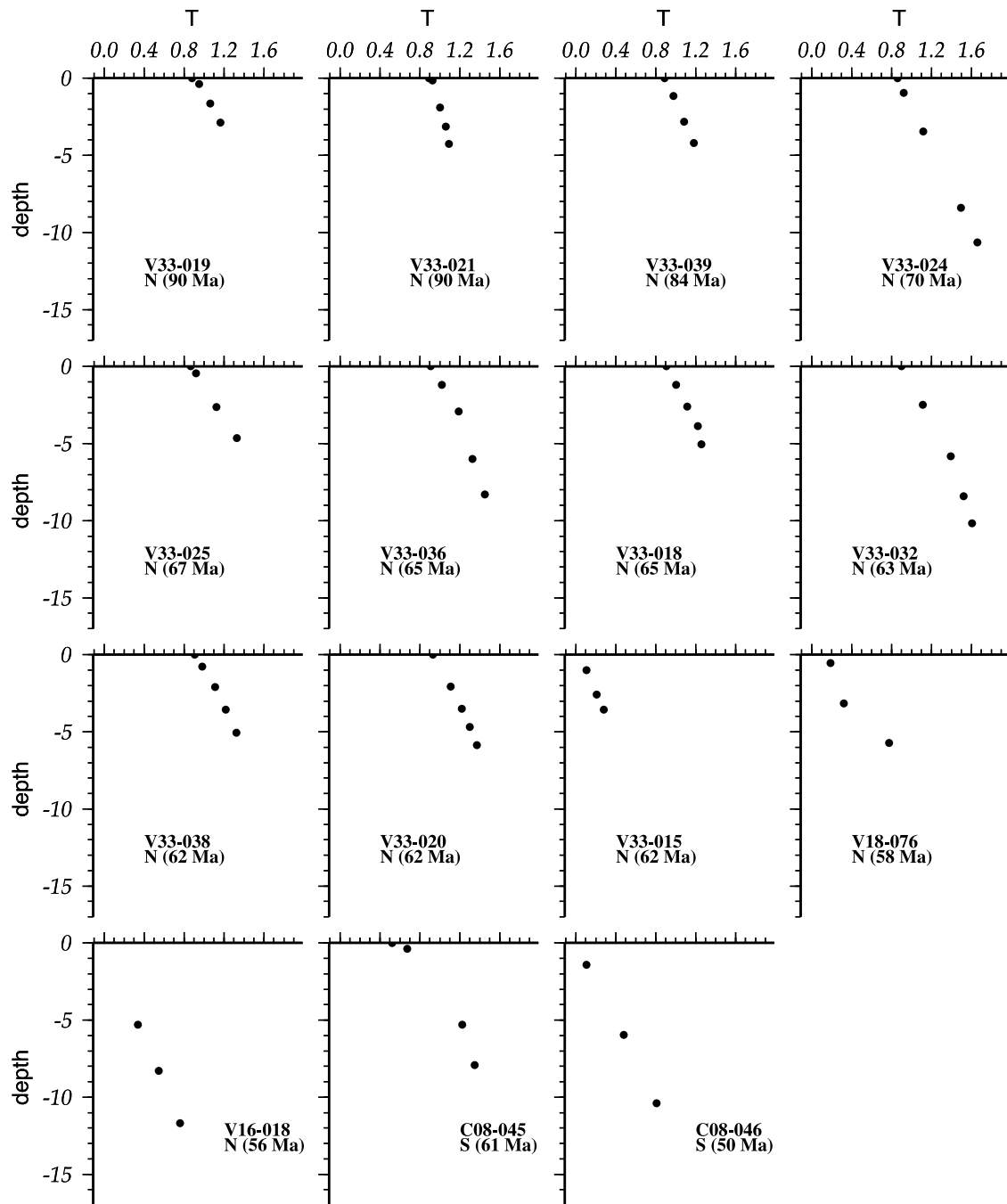**Figure 5a.** Sediment temperature (°C) profiles versus depth from the LDEO database for data points from the crust older than 43 Ma. Depths are in meters below seafloor (assuming full probe penetration). N and S indicate north and south flanks, respectively.
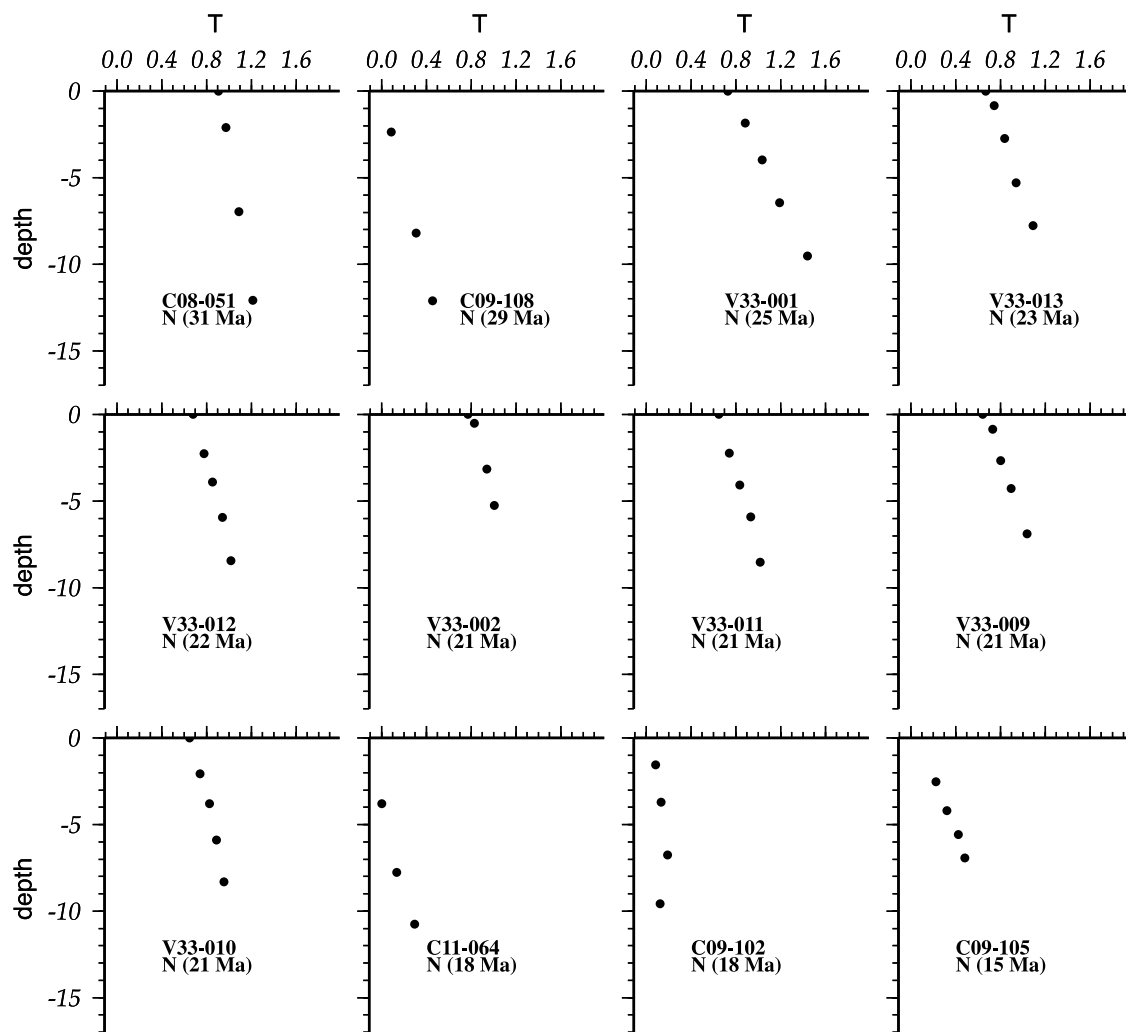
Figure 5b. Same as Figure 5a except for data points from the northern ridge flank, with crustal ages ranging between 15 and 31 Ma.

the AAD), 4 between 126° and 119°E (within the AAD), and 6 between 113°E and 86°E (west of the AAD). At each site, we conducted a local topographic survey using *Marion Dufresne*'s multibeam and 3.5 kHz echo sounder facilities over an area of about 400 km^2 centered on the coring station (Appendix A). All sites were located along the 14-Ma isochron, except MD02-2486 on the 20-Ma old crust in the southern flank. The 14-Ma isochron was chosen in consideration of three factors: (1) The theoretical variations of $T_m/\sqrt{t}$, if any, are of higher amplitude and more resolvable through young crust rather than through old crust. (2) The variability of heat flow caused by hydrothermal circulation is likely more pronounced over the younger, unsedimented crust. (3) The greatest variations in mantle temperature (Tm) are expected along isochrones younger than 25 Ma, after the onset of the numerous fracture zones that characterize the present-day AAD [e.g., *Marks et al.*, 1999].

4.2. Temperature and Conductivity Measurements

[11] We made heat flow measurements (Figures 7a and 8) using nine autonomous digital temperature probes fitted on an 18-m-long, 13-cm-diameter, gravity corer. Full penetration of 18 m was common. At some lowerings, we made multiple entries into the sediments for pogo-like thermal measurements. Because of frictional heating produced by the penetration of each probe, we recorded the temperature for 7 min and extrapolated it to infinite time to yield the ambient, equilibrium temperature in the unperturbed sediment [e.g., *Langseth*, 1965]. The equilibrium temperature was also derived using Lee's inversion method [*Lee and Von Herzen*, 1994; *Lee et al.*, 2003].

[12] The thermal conductivity of sediments was measured onboard R/V *Marion Dufresne* using the needle probe method [*Von Herzen and Maxwell*, 1959], with one measurement every 37.5 cm along the sediment core. The calculation of heat flow using such measurements, however, is susceptible to uncertainties and potential errors [e.g., *Jemsek and Von Herzen*, 1989]. (1) The shipboard needle-probe conductivity values require correction for in situ temperature and pressure at the ocean bottom. (2) The coring process probably disturbs the physical properties of the sediment sample. (3) The gravity cores collected with *Marion Dufresne* did not exceed 70% of the barrel penetration depth, except at site MD00-2375 where a full core
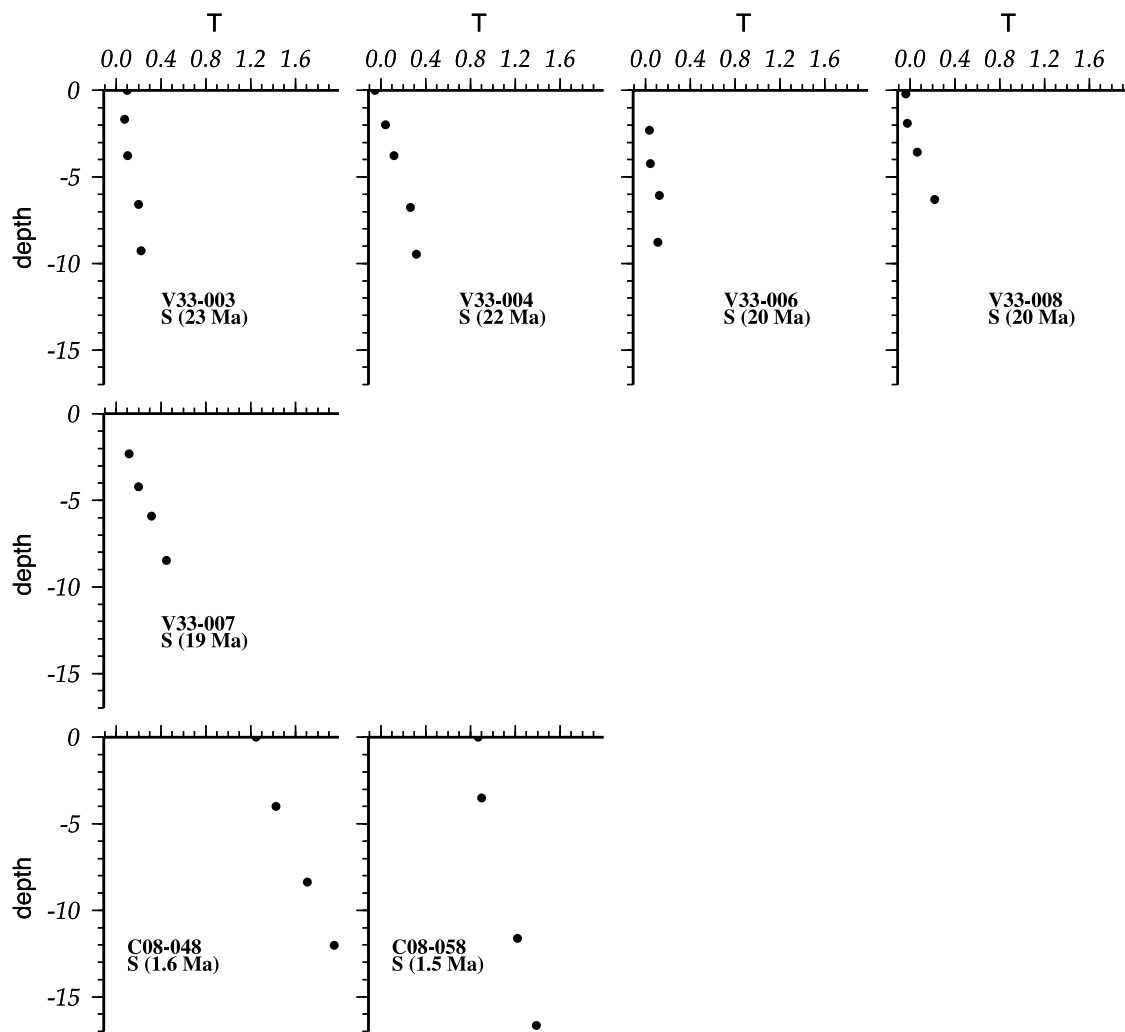
Figure 5c. Same as Figure 5a except for data points from the southern ridge flanks, with crustal ages ranging between 1.5 and 23 Ma.

was retrieved. Thus measurements on a partially recovered core do not necessarily correspond with the sediment intervals over which the geothermal gradients are determined. To avoid this shortcoming, we have also estimated the in situ horizontal thermal conductivity by modeling a cooling probe subsequent to its penetration into sediments, using the method developed by T. C. Lee [e.g., *Lee et al.*, 2003]. Table 1 displays average conductivity values; the Lee's and needle-probe values deviate less than 5% from each other. The relatively low conductivity values are probably due to high porosity (~70 to 80%) and water content in the core samples (made at Ifremer sediment core lab measurements are provided as additional material).

4.3. Heat Flow Estimates

[13] Heat flow has been estimated using two different methods. The first method consists in multiplying the average gradient by the average conductivity. The second one (described in the appendix) takes advantage of Lee's method, which provides thermal conductivity measurements collocated with thermal measurements (the classical cumulative resistance method has not been used because the conductivity measurements obtained on core samples with the needle probe method are not collocated with temperature measurements). Results are listed in Table 1. The differences do not significantly alter the conclusions of the present work.

4.4. Changes in Bottom Water Temperature

[14] Nine temperature-depth profiles exhibit departure from linearity toward the sediment surface (Figures 7 and 8): MD002363, MD00-2365-1, MD00-2365-2, MD00-2368-1, MD00-2368-2, MD00-2369-1, MD00-2369-2, MD00-2371-1, and MD00-2372-1. At these sites, the measured bottom water temperature is different by about 0.02 to 0.07°C than the "intercept temperature" from the straight line that best fits the deep temperature-depth curve. To assure the nonlinearity in geotherms at those sites have not resulted from artifact, we note that the temperature was essentially measured redundantly at "each depth" with a pair of sensors spaced 64 mm apart. The consistency in reading for each pair ruled out the possibility that sensor malfunction is a cause for the mismatch between the bottom water temperature and intercept temperature. After each station occupation, an
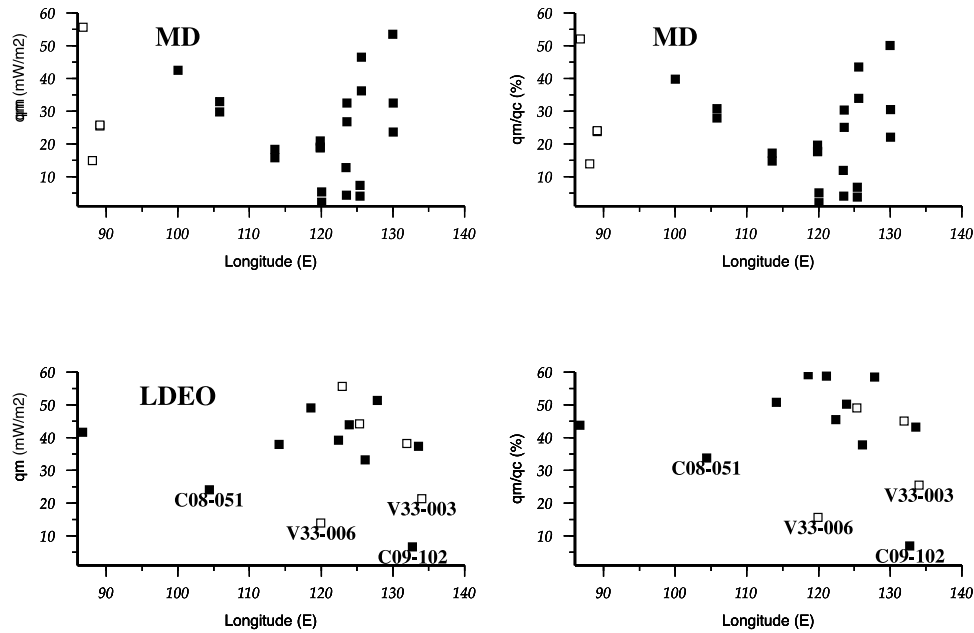
Figure 6. Variations of heat flow with longitude for *Marion Dufresne* (MD) and LDEO data sets: (left) Measured heat flow, q_m; (right) ratio of measured to predicted heat flow, q_m/q_c. The predicted heat flow is calculated using expression (1) with $k \sim 3$ W $K^{-1}m^{-1}$ and $\kappa \sim 10^{-6}$ m^2 s^{-1} and a constant, arbitrary mantle temperature of $T_m \sim 1350°C$ ($q_c \sim 410/\sqrt{age}$ mW m^{-2}). Strictly speaking, T_m decreases by $\sim 50°C$ to $70°C$ between $80°E$ and $125°E$.

onboard test of the temperature recorder indicated there was no systematic error due to thermistor calibration or drift. Local perturbations of the coring system cannot explain that departure from linearity are observed at nine stations systematically on the upper two temperature sensors.

[15] After dismissing instrumental malfunction as a cause, we consider three plausible causes or their combinations to explain the nonlinearity.

[16] 1. The temperature-depth relation can depart from the linearity in response to inhomogeneity in conductivity for a given conductive heat flux. The observed or inferred conductivity variations, however, is insufficient to account for the extent of departure.

[17] 2. The seawater could have circulated to the upper part of the sedimentary column to raise or depress the "conductive" thermal gradient. In this case, the circulation depth would have to be limited to depths penetrated by the top one or two sensors where significant nonlinearity occurs. Furthermore, it would be fortuitously unlikely that local, shallow circulation cells can cause the intercept temperatures to be consistently higher than the bottom water temperatures at those seven sites spaced tens of miles apart.

[18] 3. Finally, in the next paragraph, we explore whether a recent drop in bottom water temperature [e.g., *Davis et al.*, 2003] can cause the bottom water temperature to be less than the intercept temperature, as argued hereafter.

[19] First, we examine whether the artifact in data collection can contribute to the mismatch. If the corer has fully penetrated the sediments such that the water temperature sensor sits exactly atop the sediments, the observed difference signals a recent drop in bottom water temperature of similar magnitude. However, corer penetration is most

likely partial and the bottom water temperature will be greater than a misconstrued intercept temperature, which is contrary to our observation even if the bottom water temperature has not risen recently. Hence, in case of partial penetration, the difference is the minimum that bottom water temperature could have dropped recently. On the other hand, if the corer over penetrates the sediments, the intercept temperature will be greater than the bottom water temperature recorded with a sensor remaining above the sediments. In such case, the observed difference mentioned above would be an artifact, rather than a consequence to any suspected bottom water temperature drop. Our examination of the corer revealed no over penetration, so we are led to favor the hypothesis of a recent drop in bottom water temperature.

[20] The temperature distribution $T(z, t)$ at depth z and time t subsequent to a sudden change ΔT in the bottom water temperature can be described by

$$T(z,t) = T_0 + Gz + \Delta T erfc\left(\frac{z}{2\sqrt{\kappa_s t}}\right) \qquad (2)$$

where G is the undisturbed geothermal gradient, T_0 is the surface temperature for $t < 0$, κ_s is the thermal diffusivity of sediments, and erfc(x) is the complementary error function of argument x. If this hypothesis is correct, the thermal data are compatible with changes in bottom water temperature of $0.02°C$ to $0.07°C$ that could have occurred between one half month and 1 year before the measurement was made.

[21] The thermal probes used during the Antaus and Carhot cruises were attached with pressure sensors to

Table 1. Summary of Thermal Measurements From the Southeast Indian Ridge Flanks between 70°E and 140°E[a]

Latitude	Longitude	Label	Water Depth, m	Age, Ma	Needle Probe Gradient, K km^{-1}	Needle Probe Condition, W m^{-1} K^{-1}	Needle Probe HF, mW m^{-2}	Lee Gradient, K km^{-1}	Lee Condition, W m^{-1} K^{-1}	Lee HF, mW m^{-2}
					LDEO					
−56,1	131,917	V33-4	4402	22.2	38	0.63	24			
−56,217	134,017	V33-3	4130	22.8	21	0.63	13			
−54,483	119.933	V33-6	4029	20.2	14	0.64	9			
−54.467	122.9	V33-7	4514	19.7	56	0.63	35			
−54.533	125.333	V33-8	4679	19.8	44	0.68	30			
−51.083	129.967	C8-58	3442	1.5	37	0.88	33			
−45.417	121.117	C9-105	4400	14.9	61	0.78	47			
−45.017	132.75	C9-102	4675	17.6	7	0.78	5			
−44.767	92.417	C8-48	3219	1.6	65	0.99	64			
−44.2	133.583	V33-2	4708	21.3	37	0.76	28			
−43.5	118.517	V33-13	4423	23.3	49	0.73	36			
−43.5	122.433	V33-12	4728	21.5	39	0.69	27			
−43.5	123.917	V33-11	4543	20.9	44	0.70	31			
−43.5	126.1	V33-10	4684	20.7	33	0.70	23			
−43.5	127.8	V33-9	4816	20.8	51	0.67	34			
−43.067	134.367	V33-1	4905	25.3	72	0.75	54			
−41.367	114.133	C9-108	4396	28.7	38	0.74	28			
−39.383	104.367	C8-51	4429	31.5	24	0.79	19			
−37.983	86.65	C11-64	3766	17.6	42	1.11	46			
					Antaus					
−45,452	123.455	MD002362	4740	13	11.8	0.68	8	16.9	0.72	13
−45,443	123.536	MD002363	4520	13	7.8	0.73	6	5.8	0.71	4
−45,520	123.549	MD002364-1	4380	13	31.9	0.72	23	39.6	0.71	27
−45,522	123.561	MD002364-2	4390	13	39.6		29	44.8	0.73	32
−44,916	125.572	MD002365-1	4700	14	64.9	0.70	45	69.8	0.66	46
−44,925	125.581	MD002365-2	4700	14	47		33	52.8	0.71	36
−44,944	125.426	MD002366-1	4450	14	11.6	0.79	9	5.3	0.76	4
−44,950	125.429	MD002366-2	4450	14	10.6		8	9.8	0.71	7
−45,894	129.963	MD002367-1	4380	14	66.8	0.8	53			
−45,968	130.018	MD002368-1	4500	14	45.9	0.76	35	47.2	0.71	33
−45,973	130.020	MD002368-2	4490	14	37.4		28	37.2	0.63	24
−45,279	120.027	MD002369-1	4430	14	8	0.72	6	3.1	0.69	2
−45,284	120.038	MD002369-2	4430	14	7.9		6	6.7	0.74	5
−45,383	119.866	MD002370-1	4240	14	20.8	0.79	16	27.0	0.70	19
−45,384	119.865	MD002370-2	4230	14	22		17	28.3	0.74	21
−45,386	119.870	MD002370-3	4215	14	21.3		17	26.3	0.73	19
−45,398	113.492	MD002371-1	4120	14	22.9	0.78	18			
−45,404	113.495	MD002371-2	4120	14	26.8		21			
−44,137	105.825	MD002372-1	3840	14	51.3	0.88	45	55.4	0.59	33
−44,145	105.828	MD002372-2	3800	14	45.7		40	46.3	0.64	30
−43,481	99.988	MD002373-2	3753	14	48.3	0.96	46			
−45,713	86.750	MD002375	3500	14	69.8	0.80	56			
					Carhot					
−47,003	89.112	MD022486-1	3380	20	33.4	0.76	25			
−47,003	89.110	MD022486-2	3406	20	33.8		26			
−46,478	88.022	MD022487	3489	14	21.0	0.70	15			

[a]Crustal age is <42 Ma. Conductivity and heat flow were computed using the Lee's method for a number of sites collected during the Antaus cruise. The listed results allow comparisons between two different methods. A comprehensive table including all temperature and conductivity data from the study area (70°E−140°E/30°S−70°S) is available in the auxiliary material. HF, heat flow.
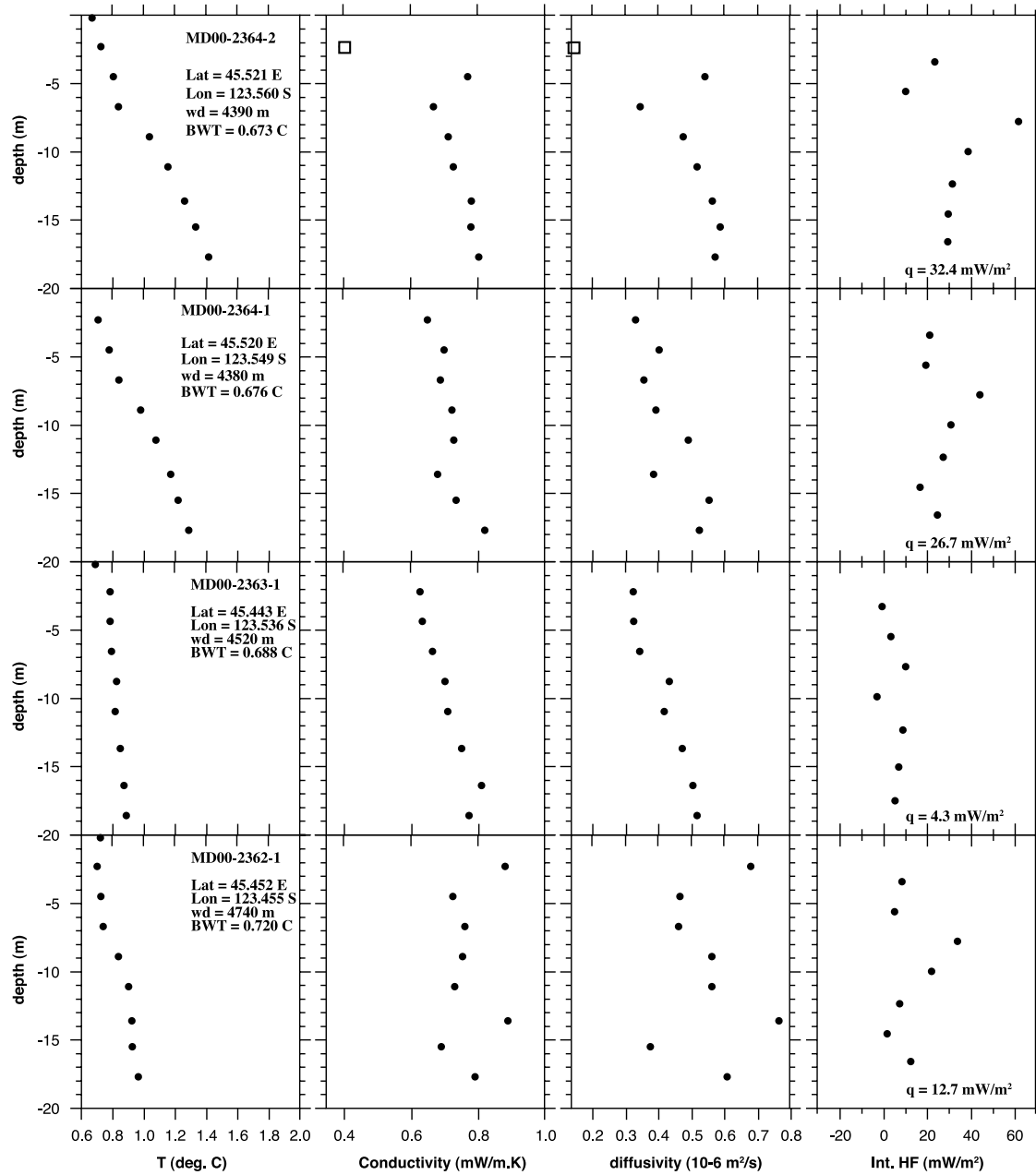
Figure 7. Thermal measurements obtained with R/V *Marion Dufresne* on the northern flank of the SEIR (see Table 1). The equilibrium temperature, the thermal conductivity, and the thermal diffusivity of the sediments were obtained by inverse modeling the first minute of the cooling curve (temperature versus time) after the penetration of the core.
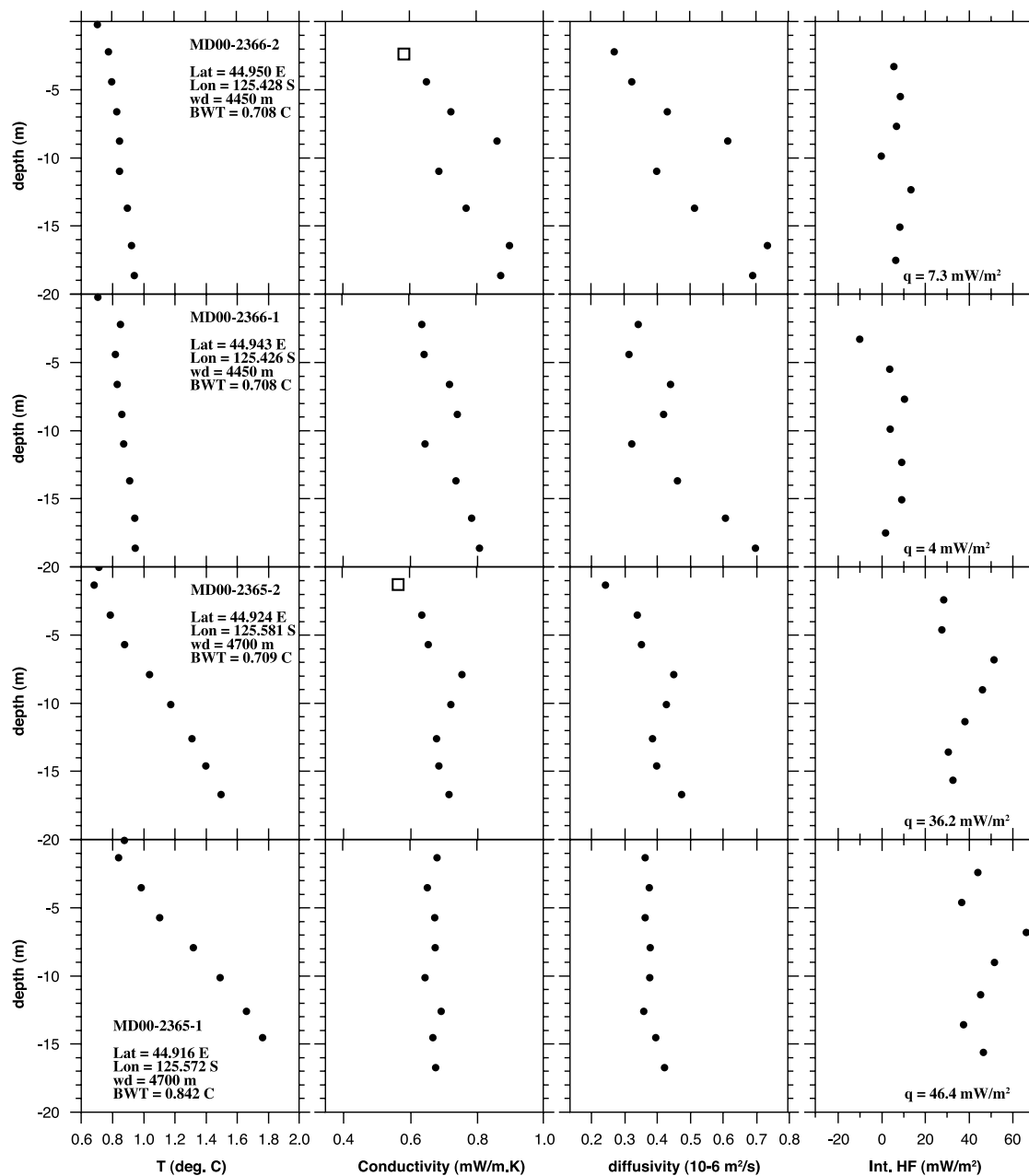
Figure 7. (continued)

measure pressure and hence temperature-depth profiles within the water column. These profiles show that the bottom water is colder by 0.1 to 0.2°C within or near the AAD (Figure 9). A current meter mooring at 4525 m depth at 47°29.8′S and 124°04.6′E within the AAD recorded a mean flow of 3.5 cm s^{-1} in the northwest direction, consistent with the inferred transfer of cold water from the south into the South Australian Basin [*Rodman and Gordon*, 1982; *Jacobs et al.*, 1974]. The small-scale bottom roughness within the AAD probably affects the turbulent eddy diffusivity [*Mauritzen et al.*, 2002] and the mixing process through drag on bottom currents at length scales shorter than ∼10 to 20 km [e.g., *Kunze and Llewellyn Smith*, 2004]. Local changes in bottom water temperatures can thus occur

at various time and spatial scales, causing the observed change in temperature gradient near the sediment/water interface.

5. Heat Flow Data Analysis

5.1. Lateral Heat Transfer by Channelized Water Circulation Within the Upper Crust

[22] The seafloor in the AAD is very rugged and the sediment cover is patchy. The discontinuous sediment cover allows hydrothermal fluid to vent through the fractured outcrops of igneous basement. The hydrothermal circulation under the sediment cover can effectively remove heat energy to lower the conductive heat flow (Table 1), which can be measured only in the sediments. The fact that the
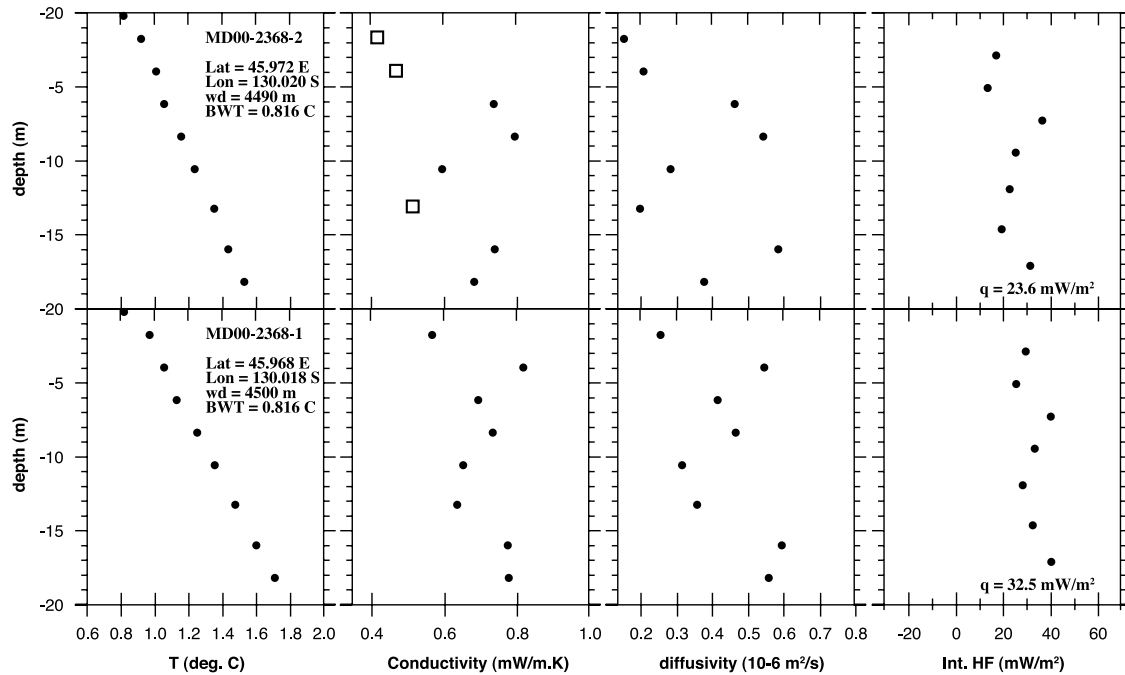
Figure 7. (continued)

measured heat flux is much less than the value expected of a conductive cooling model lends credence to a claim of significant advective heat transfer in the upper crust (Figure 6).

[23]   To explain low heat flow anomalies from the Brazil basin, *Langseth and Herman* [1981] proposed a simple heat exchanger model, in which cold seawater penetrates into the upper, permeable crustal layer through faults and flows laterally until it discharges at the seafloor. This model has been shown to be very efficient in removing heat from the ocean crust in many case studies [e.g., *Davis et al.*, 1999]. *Fisher and Becker* [2000] showed that it is possible to use a "channelized fluid flow model" to reconcile permeability measurements in the uppermost oceanic crust and heat flow data. In this model, the measured heat flow q_m decreases with increasing distance x from the water intake as

$$q_m(x) = q_c \left[1 - e^{x\left(\beta/2 - \sqrt{\frac{\beta^2}{4} + \frac{ks}{k_b h_b h_s}}\right)} \right] \qquad (3)$$

where $\beta = u\rho_w C_p/k_b$, u is the horizontal flow velocity, k_b is the basement thermal conductivity, and ρ_w and Cp are the density and heat capacity of seawater, respectively, and q_c is the theoretical, conductive heat flow. *Langseth and Herman* [1981] noted that the measured heat flow, $q_m(x)$ and q_c, can be substituted for $T(x)$ and T_∞, where T_∞ is the temperature that would be expected at the base of the aquifer in the absence of water circulation. The horizontal fluid velocity can be expressed as a function of the pressure gradient using a form of Darcy's law

$$u = -\frac{\xi}{\mu}\frac{\Delta P}{\Delta x} \qquad (4)$$

where ξ is the medium permeability, μ is the fluid viscosity, and ΔP is the fluid pressure difference over Δx, which represents the lateral distance between the intake and the outlet of seawater circulation. *Fisher and Becker* [2000] write ΔP as a function of the fluid density difference $\Delta\rho$ between downflow and upflow zones:

$$\frac{\Delta P}{\Delta x} = \frac{\Delta\rho}{\Delta x} g(h_s + h_b) \qquad (5)$$

where h_s and h_b are the thickness of the sediment layer and the permeable basement layer, respectively, and g is the gravitational acceleration. The density difference is proportional to α, the fluid thermal expansion coefficient

$$\Delta\rho = -\alpha\rho_w T_\infty \qquad (6)$$

[24]   We have used two different values for Δx (12.5 and 25 km) and two different values for h_b ($h_b = 500$ m and 1000 m; $h_s = 150$ m), with a set of basement permeabilities varying from 10^{-13} to 10^{-9} m^2 (Figure 10). With $\mu = 1.3 \times 10^{-3}$ kg m^{-1} s^{-1}, the model indicates that heat removal by lateral flow of water is 50% that of lithospheric cooling at distances more than 10 km away from the downflow intake zone if the bulk permeability is greater than $\sim 10^{-10}$ m^2 and $h_b = 1000$ m, or if the permeability is greater than $\sim 10^{-9}$ m^2 and $h_b = 500$ m. These orders of magnitude are consistent with the findings by *Fisher and Becker* [2000]. The model, however, is best used where there is dominantly sediment-covered basement, with a small number of outcrops (or a small area of basement exposure), and a one-dimensional flow path. In the present study area, there is mostly outcrop across huge areas and a few sediment patches. It is hence
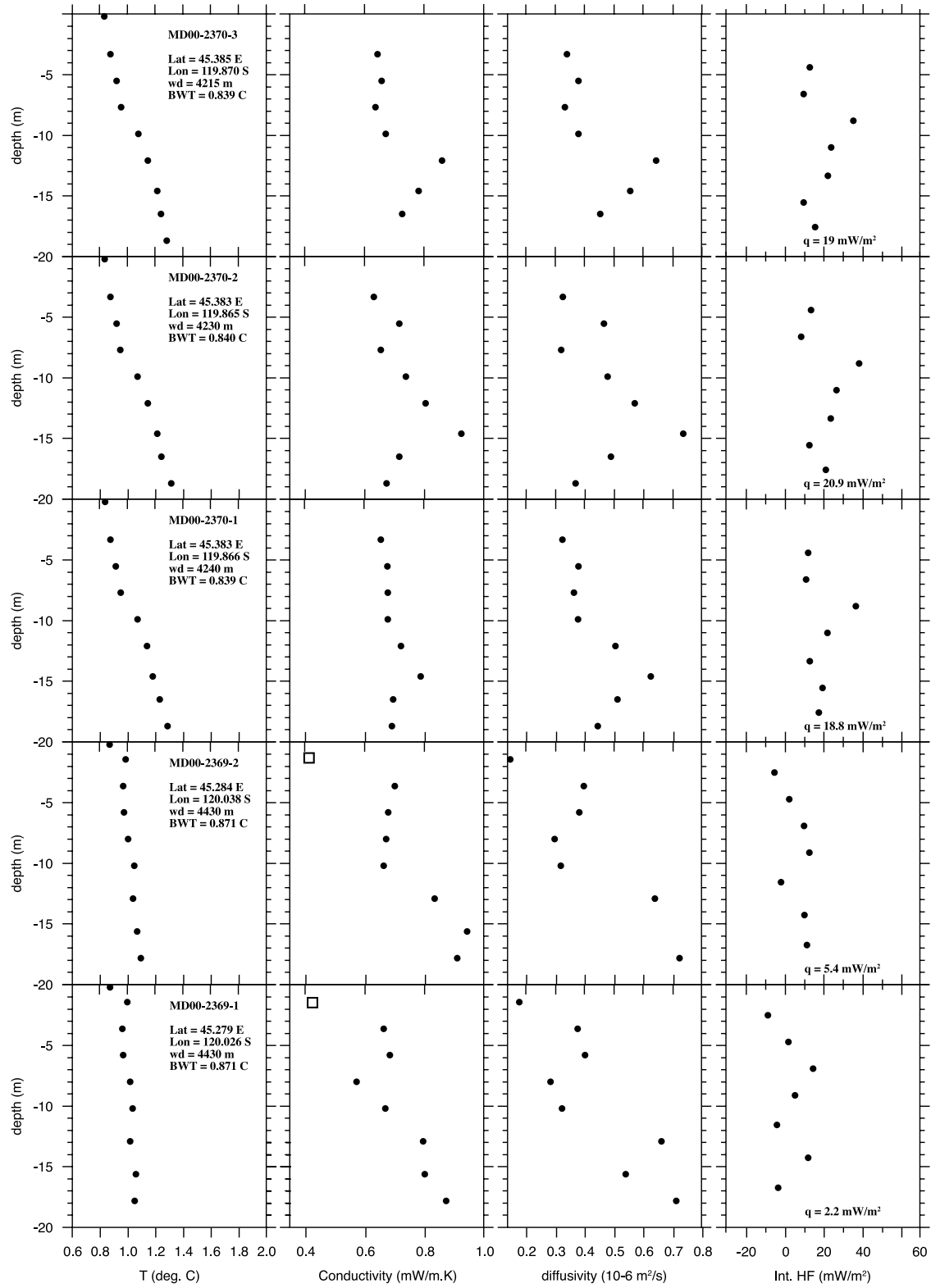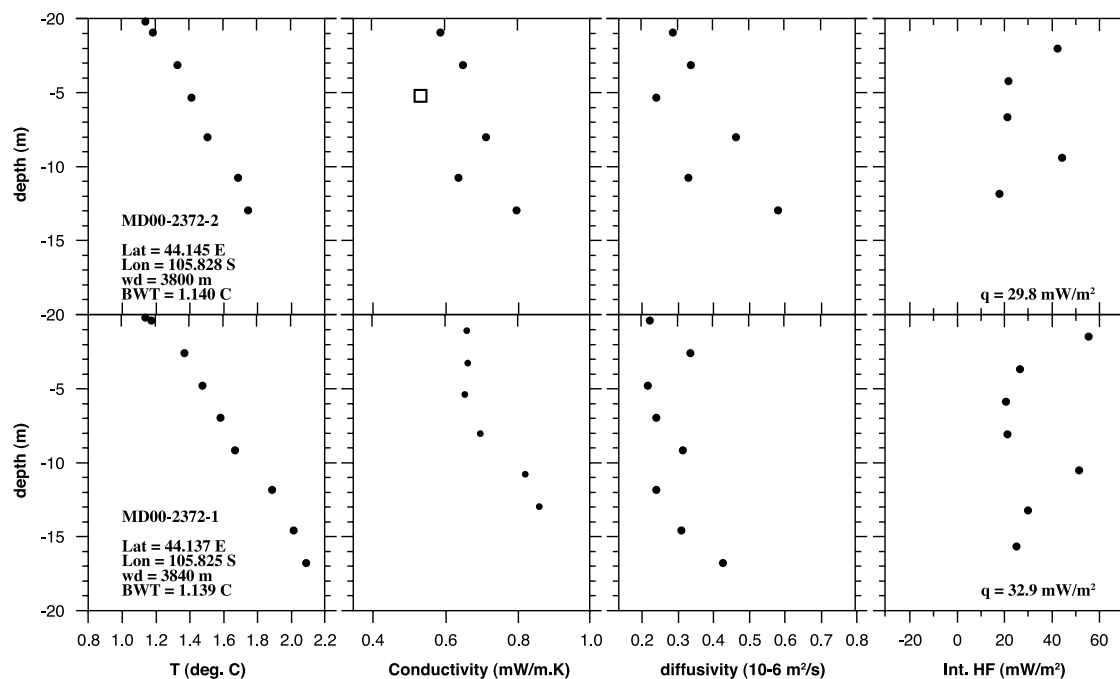
Figure 7. (continued)

Figure 7. (continued)

5.2. Possible Cooling by Vertically Channelized Seawater Circulation Along Faults

[25] Because the AAD seafloor is poorly sedimented and highly fractured with ridge-parallel and ridge-perpendicular faults, we propose that other effects, specific to the study area, could also play a role to explain the low heat flux. For instance, consider sites MD00-2362 and MD00-2363, located in or near an elongated trough, deeper than 4800 m. This trough is likely a surface expression of a ridge parallel fault (Appendix A). At these two sites, conductive heat flow values as low as 12 and 4 mW m^{-2} were measured, respectively (Figure 8). Fed continuously by cold seawater into the fault zones, the circulating water could cool a substantial fraction of the crust (Figure 11).

[26] It is also interesting to note that the heat flux variability within the AAD is – from a statistical point of view, higher on 14 Ma crust than on 22 Ma old crust. On ~14 Ma old crust, there are 12 data points with heat flux ratio (q_m/q_c) ranging between 4% and 45%. On 22 Ma crust, the heat flux is small but the data dispersion is surprisingly small (between 35% and 55%). Although there are a very limited number of points in the database, we think that this could have something to do with crustal cooling by vertically channelized water circulation along faults.

[27] This hypothesis is not farfetched, considering that a significant permeability contrast of 3 to 5 orders of magnitude exists at continental faults between the ''damage zones'' and the surrounding crustal rock [e.g., *Ben Zion et al.*, 2003; *Lockner et al.*, 2000]. Under the seafloor, water could penetrate not only through the main active fault but also through parallel subsidiary faults, each having a dam-

age zone of a few hundreds meters wide and a common root base at depth. Here, we postulate that this root could be located within the lower crust. The occurrence of intraplate earthquakes within the AAD suggests that the oceanic crust fractures frequently, which may maintain high permeabilities near intraplate fault zones. The fracturing could have been ongoing over the last 25 Ma.

[28] Because of self-sealing by chemical deposition along the flow path, water circulation may not persist to a steady state. Self-sealing, however, would be a problem only if the fluid were heated significantly after entering the crust. For deep circulation that chills the crust as proposed here, there would be little or no sealing. For deep circulation at higher temperatures, a plugged fault can be rejuvenated for renewal of water flow by crustal fracturing. If a fault zone consists of a number of parallel faults with a common root at depth, there could be a ''perpetual'' pattern of alternate closing and opening of water circulation through various subsidiary faults. Within the AAD area, the faulting pattern of criss-crossing ridge-parallel and -perpendicular faults could allow the entire crust and perhaps the upper mantle to cool effectively by seawater circulation.

6. Conclusion

[29] In the absence of the detailed documentation of basement topography and sediment thickness distribution, it is difficult to interpret the data quantitatively. Rugged basement topography and strong bottom currents have resulted in a patchy sediment cover, however, and lateral heat transfer by horizontally channelized water flow within the upper crust is likely to be the primary cause of low heat flow throughout the AAD. Low regional heat flow is known to occur in other areas
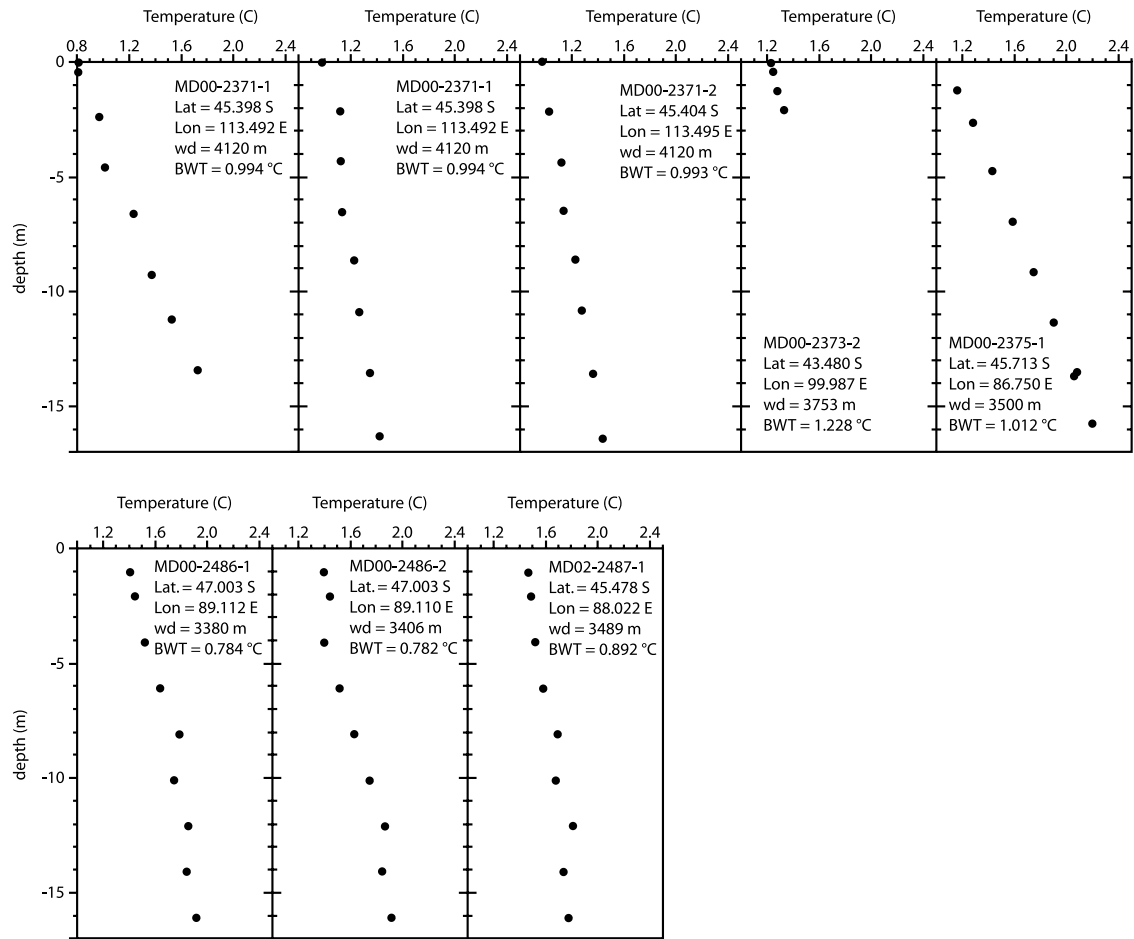
Figure 8. Temperature profiles obtained with R/V *Marion Dufresne* on the southern flank of the SEIR (see Table 1). The sediment equilibrium temperature was obtained using the classical method [*Langseth*, 1965].
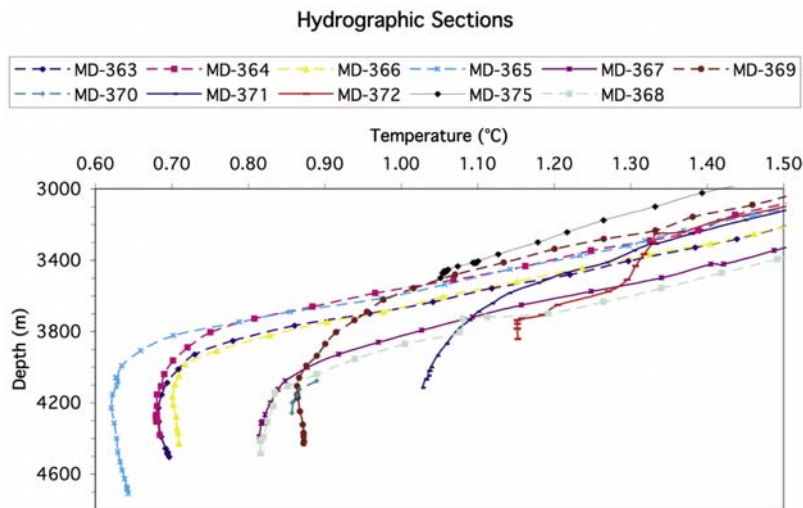

Figure 9. Hydrographs in the water column [after *Labails*, 2001]. Each thermal probe is attached with a pressure transducer for depth measure.
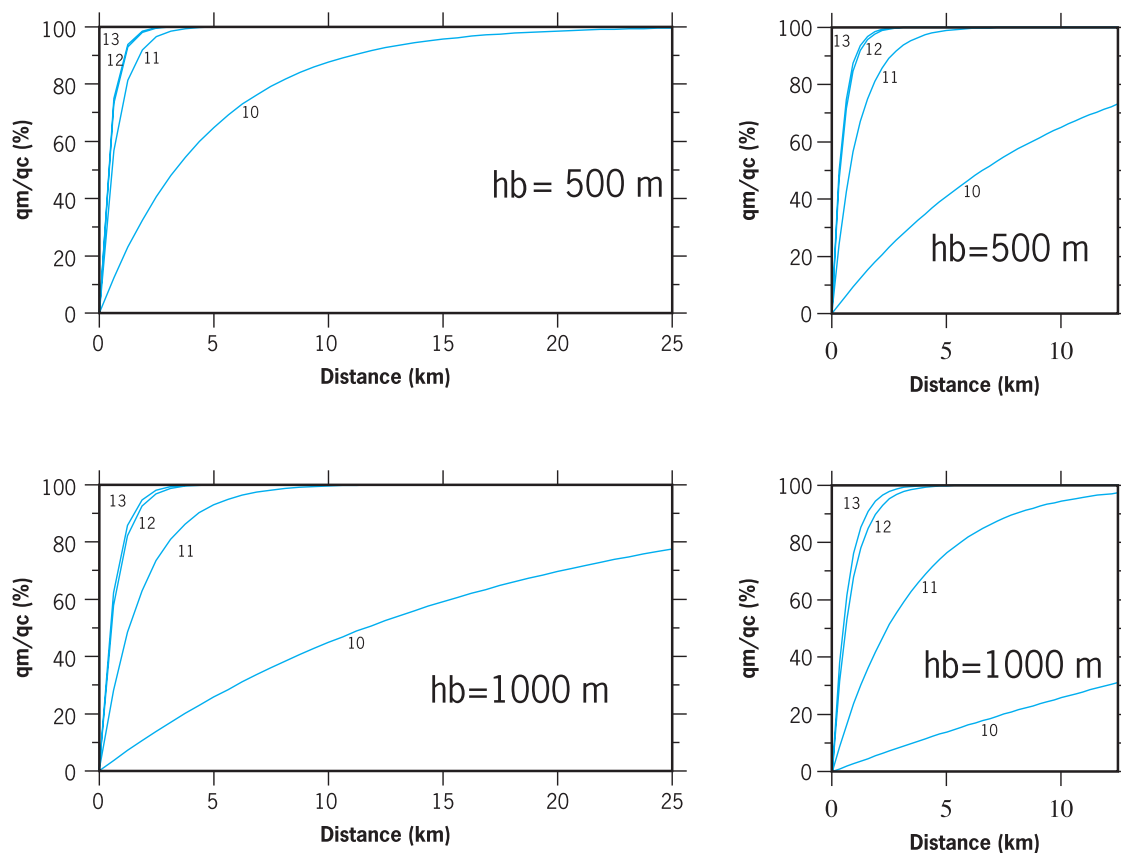
Figure 10. Model results showing thermal effects of water flowing laterally within the upper permeable crustal layer, based on work by *Langseth and Herman* [1981] and *Fisher and Becker* [2000]. Surface heat flow as normalized by q_c is plotted versus distance from water intake. Δx is the half distance between two successive zones of water upflow ($\Delta x = L_{max}/2$). Two cases are displayed, for $\Delta x = 12.5$ km and 25 km, respectively. Different values of permeabilities (k) within the fault are considered, from 10^{-13} to 10^{-10} m^2. Curve labels indicate $-\log(k)$. The permeable layer thickness (h_b) is equal to (top) 500 m and (bottom) 1000 m. Viscosity of water (μ) is assumed to be equal to 1.3×10^{-3} kg m^{-1} s^{-1}.

with rugged seafloor and discontinuous sediment cover [e.g., *Fisher and Becker*, 1995; *Davis et al.*, 1997].

[30] In addition to being discontinuously sedimented, the AAD area is highly fractured, with ridge-parallel and -perpendicular faults. Seawater could circulate along numerous faults, possibly down to the base of the crust. So, in addition to the heat removal by horizontally channelized fluid flow, circulation of water along the numerous vertical fault zones can further reduce heat flow. This process has yet to be directly documented. Confirmation would require systematic, closely spaced heat flow measurements along and across fracture zones, with detailed seismic mapping of sediment thickness. With these constraints, quantitative modeling of the heat flow distribution could lead to a better understanding of hydrothermal circulation in the ridge flanks and within fracture zones.

Appendix A: Description of R/V *Marion Dufresne* Heat Flow Sites

A1. Site 1, East of the AAD Near 45°57′S, 130°E

[31] This site is located near ODP Drill Site F1159, 150 km to the east of the fracture zone that delineates the eastern boundary of the AAD (Figure A1). The ODP site was located in a valley containing 145 m of sediments. The topography is marked by a succession of abyssal hills and valleys, oriented N100° over an area about 8 km wide. The hills reaching depths of about 4200 m are demarcated by highly reflective, prominent escarpments that bound elongated troughs about 1 km wide, 10 km long, and 4,800 m deep. One core (MD00-2368) was taken about 4 km away from the axis of a trough. The two thermal measurements at this core site exhibit linear thermal profiles (with average thermal gradient of about 46 and 37 K km^{-1}, respectively), except near the sediment surface.

A2. Site 2, Within the AAD, Near 44°55′S, 125°30′E

[32] Located within segment "B4" of the AAD, site 2 is characterized by 5,000 m deep, N100° oriented narrow troughs (<3 km wide and 10 to 15 km long), alternating with 2- to 4-km-wide abyssal hills with their tops at 4300 m depth (Figure A2). One core (MD00-2365) came from a relatively flat area, 8 km away from the nearest trough. Two thermal measurements yielded an average temperature gradient of 65 and 47 K km^{-1} each. Another core (MD00-2366) was retrieved less than 4 km away from a deep
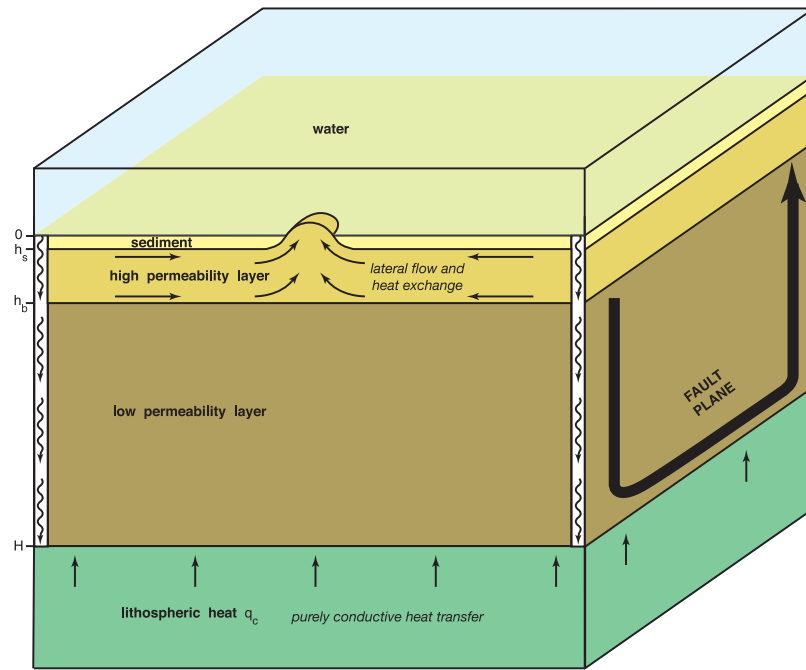
Figure 11. Cartoon for the hydrological model. Seawater circulation within the upper crustal layer is horizontal and controlled by basement topography. Within the lower crustal layer, seawater may occur along faults planes (ridge-parallel and ridge-perpendicular), down to the base of the crust.
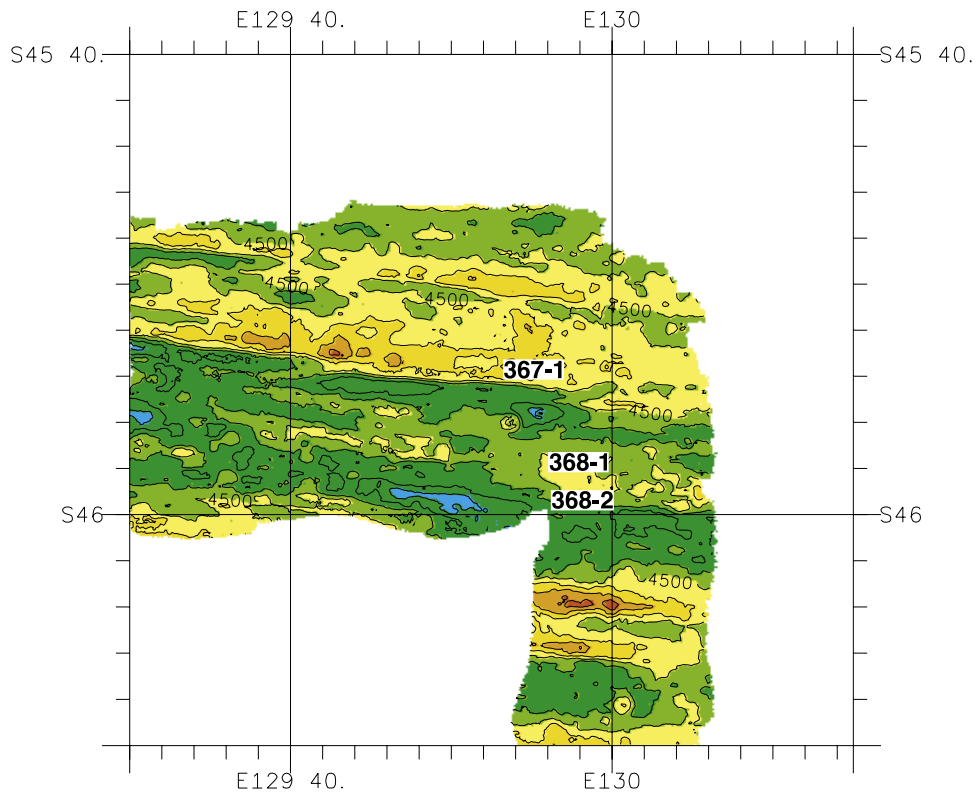

Figure A1. A swath of bathymetry collected with R/V *Marion Dufresne* during the Antaus Cruise (see sites description in Appendix A) showing bathymetry in the vicinity of sites 367-1, 368-1, and 368-2.
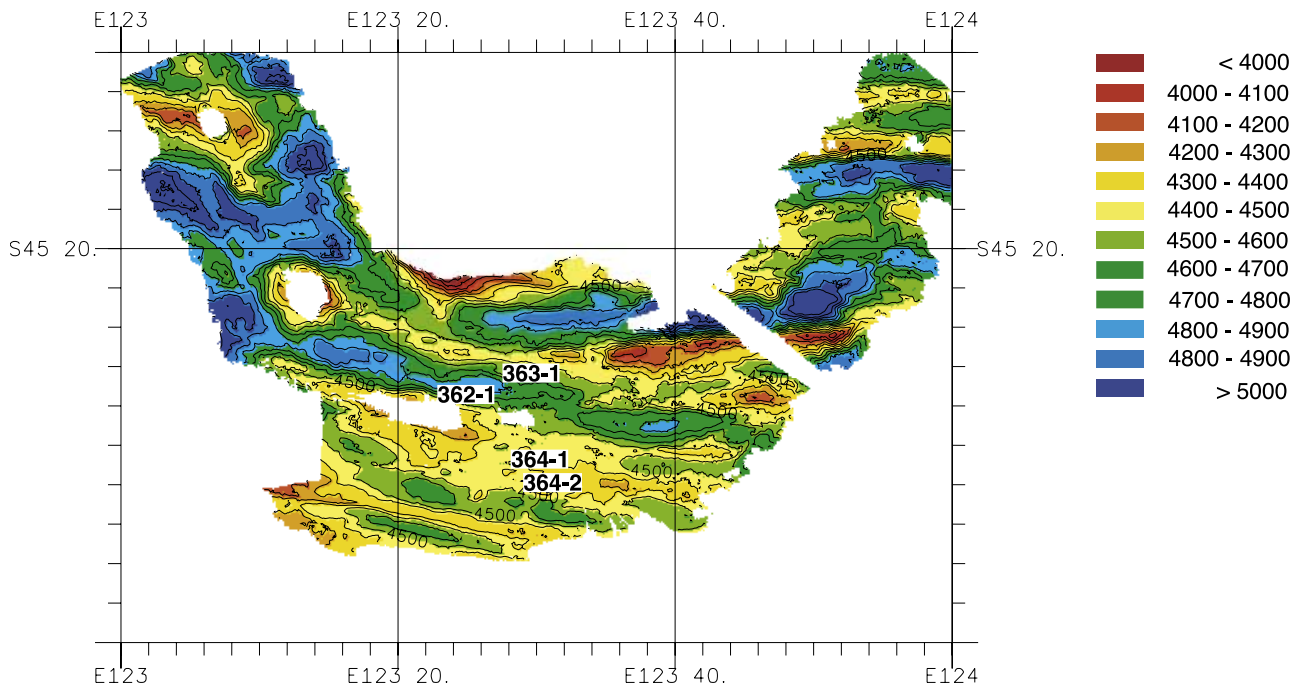
Figure A2. Same as Figure A1 except for bathymetry in the vicinity of sites 362-1, 363-1, 364-1, and 364-2. The measured values of heat flow (13 and 4 mW m^{-2}) over the topographic lows (MD00-362 and MD00-363) are smaller than those (32 and 44 mW m^{-2}) found at site MD00-2364 over topographic highs.
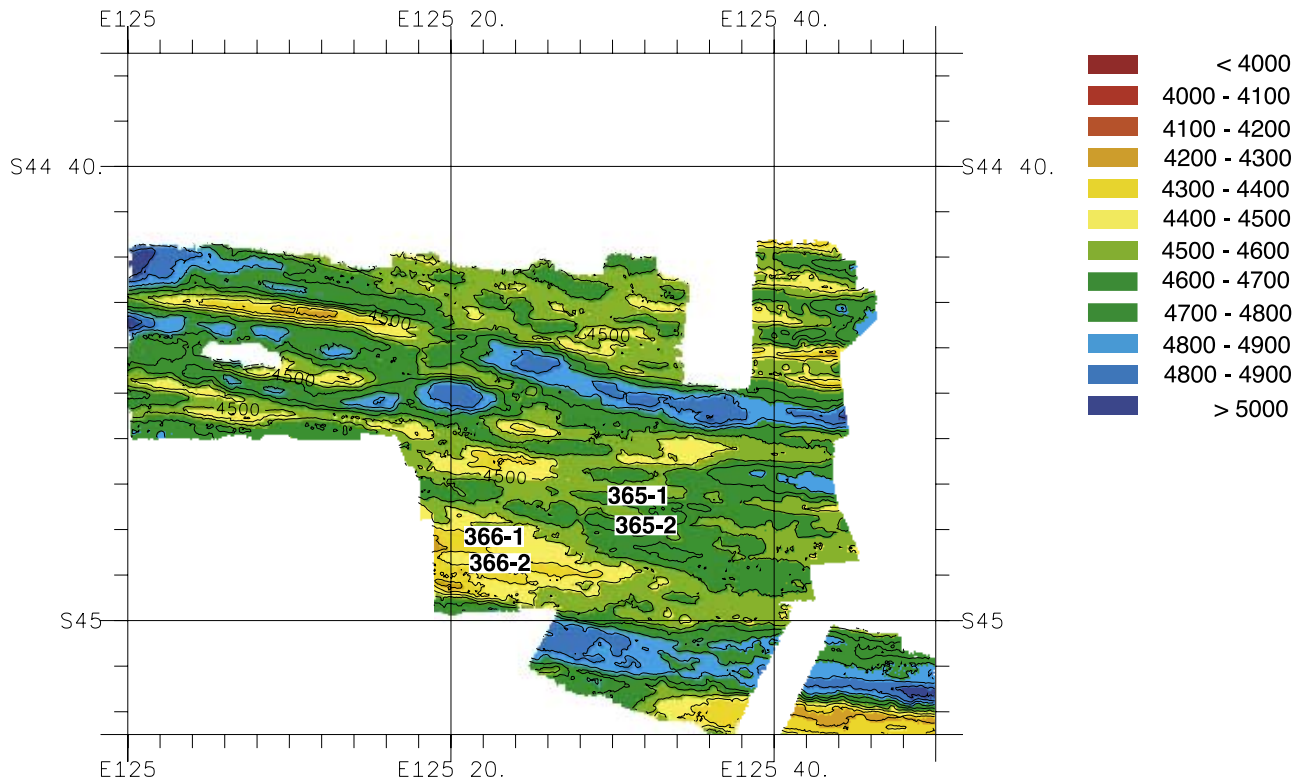

Figure A3. Same as Figure A1 except for bathymetry in the vicinity of sites 365-1, 365-2, 366-1, and 366-2. The measured values of heat flow (4 and 7 mW m^{-2}) over the topographic high (MD00-366) are smaller than those (46 and 36 mW m^{-2}) found at site MD00-2365 over in the topographic lows, opposite to the trend in Figures A2 and A4.
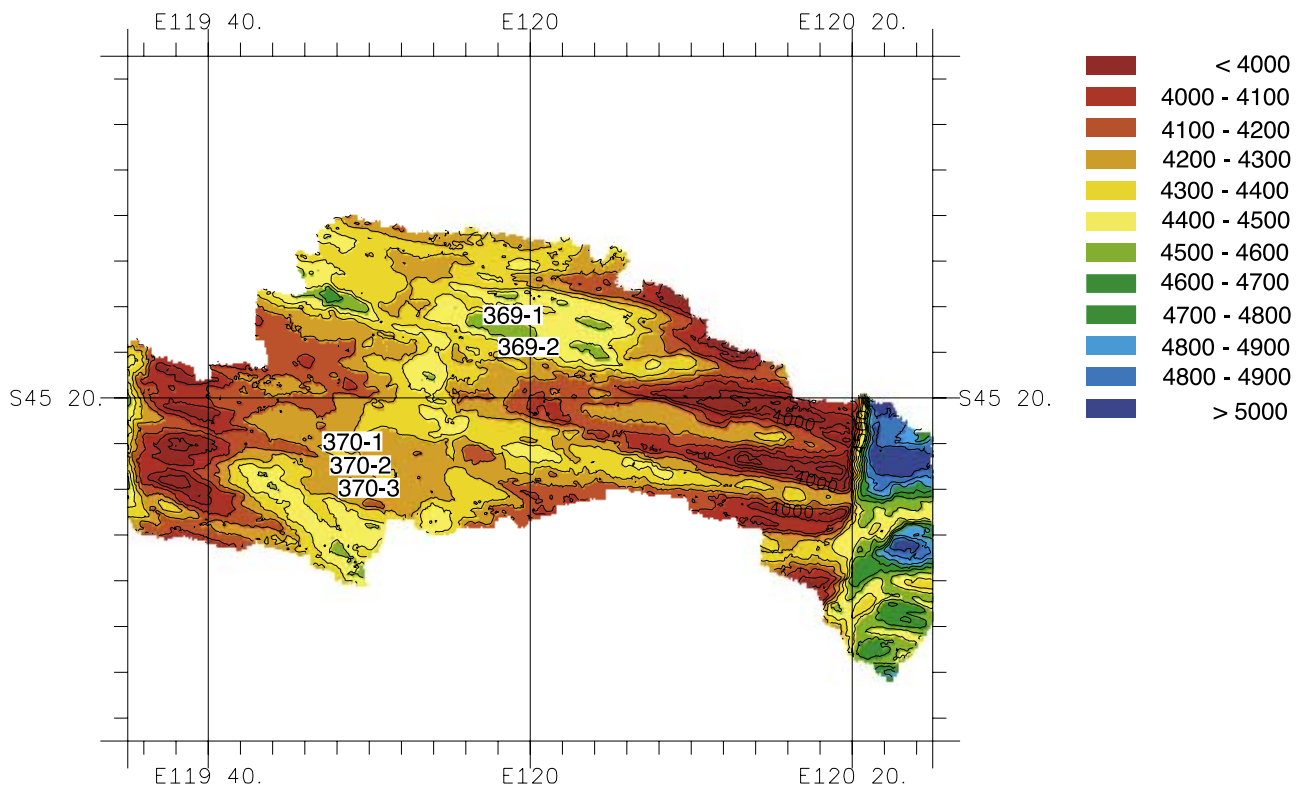
Figure A4. Same as Figure A1 except for bathymetry in the vicinity of sites 369 (369-1 and 369-2) and 370 (370-1, 370-2, and 370-3). The measured values of heat flow (2 and 5 mW m^{-2}) over the topographic lows (MD00-369) are smaller than those (19, 21, and 19 mW m^{-2}) found at site MD00-2370 in the topographic highs.

trough, probably near an escarpment. The two thermal gradients measured near the latter core site were much lower (12 and 11 K km^{-1}, respectively).

A3. Site 3, Within the AAD, Near 45°27′S, 123°27′E

[33] Site 3 was located on the 14-Ma crust, within segment "B2" of the AAD, at about middistance (more than 60 km away) from two major fracture zones (Figure A3). The seafloor is very rough, characterized by lens-shaped abyssal hills oriented N100°, 20 to 30 km long and 7 to 8 km wide and separated by 5-km-wide valleys. The hills are separated by prominent escarpments from elongated troughs with depths deeper than 5000 m. Two cores (MD00-2362 and MD00-2363) were taken near a trough. The site yielded two consistent temperature gradients of about 8 mK m^{-1} each. Whereas, two measurements at the third core station (MD00-2364) atop a nearby abyssal hill yielded much greater temperature gradients of 32 and 40 K km^{-1} each.

A4. Site 4, Western Edge of AAD, Near 45°20′S, 120°E

[34] Located near the western limit of the AAD (about 25 km to the west of a fracture zone that crosses the ridge axis near 120°30′E), site 4 exhibits a rough seafloor dotted with a few fossil structures that probably have resulted from axial reorientations during the last 14 Ma (Figure A4). The area is characterized by a series of alternating abyssal hills (4 km wide, 15 km long, below 3,800 m depth) and narrow

valleys. One core station (MD00-2369), from a depression on the flank of an abyssal hill, yielded low-temperature gradients of about 8 K km^{-1}. A second core site (MD00-2370) atop a topographic high yielded three relatively higher thermal gradients of about 21 K km^{-1}.

A5. Site 5, Near 45°24′S, 113°30′E

[35] Bordered by sharp escarpments, the abyssal hills around site 5 are 7 to 9 km wide. One core (MD00-2371) was recovered from a relatively flat depression, about 4 to 5 km from the nearest escarpment. Two modest temperature gradients were measured, 23 and 27 K km^{-1}, respectively.

A6. Site 6, Near 44°08′S, 105°49′E

[36] Site 6 was located near two existing seismic lines ELT49 and ELT50 (http://www.marine-geo.org/seislink/) which revealed a sedimentary lens of 200 to 300 m thick. One gravity core (MD00-2372) was taken from a 3800-m-deep flat area, which turned out to be underlain by indurated sediments in a channel incised by bottom currents. The corer bent during the second pogo penetration. Two temperature gradients were obtained, 51 and 46 K km^{-1}.

A7. Site 7, Near 43°30′S, 100°E

[37] This site was located on a 14-Ma old crust, in an area where the Eltanin seismic sections (http://www.marine-geo.org/seislink/) exhibit a nonuniform, 300- to 400-m-thick

sediment cover that drapes over the topographic highs. The seafloor is characterized by abyssal hills, oriented N45°, at depth less than 200 m. According to the classification of *Sclater et al.* [1976], the site falls into category "B" of seafloor relief. One gravity core (MD00-2373) was taken from a 3,800 m deep, flat area underlain by indurated sediments. The corer bent at the first penetration. One temperature gradient was obtained, 48 K km^{-1}.

A8. Sites 8, 9, and 10 on the Southern Flank of the SEIR

[38] These sites were selected for their high sedimentation rates and relevance for paleoceanographic studies. Core MD00-2375 (17.5 m long) was taken from a relatively flat area, almost uniformly covered by a sediment blanket over 200 m thick, based on information provided by a near-by seismic line (http://www.marine-geo.org/link/data/image/seismic_reflection/ELT47/panels2/011.jpg). The site yielded a linear profile with a temperature gradient of 70 mK m^{-1}. Temperature gradients as low as 33 and 21 K km^{-1} were measured at core sites MD02-2486 and MD02-2487, respectively.

Appendix B: Thermal Conductivity and Heat Flux Measurements Using Lee's Method

B1. Thermal Conductivity

[39] The in situ horizontal thermal conductivity has also been estimated by modeling a cooling probe subsequent to its penetration into sediments [*Lee et al.*, 2003]. The idea of using the cooling history of a friction-heated probe for estimating in situ conductivity has floated around ever since the first set of marine heat flow measurements were made [*Bullard*, 1954]. However, it was not feasible to test the idea with analog data or coarsely sampled digital data. *Lee and Von Herzen* [1994] first demonstrated the feasibility with a trial-and-error nonlinear inversion. A decade later, *Lee et al.* [2003] improved the methodology with finely sampled data and by incorporating a genetic algorithm (GA) to initialize input parameters for inverse modeling (IM) the first minute record of a cooling probe (60 points at 1 s sampling intervals), as simulated by finite element analysis (FE). (Here, the first 3 min of records was used for 36 points at 5 s sampling intervals.) The model in situ conductivity values in their test cases agree with the corresponding needle-probe values to within the measurement errors for needle probes.

[40] Slightly modified for modeling efficiency, the method of *Lee et al.* [2003] was adopted here. Each run of GA-IM process yields a least RMS for misfit (model misfit) and a corresponding set of thermal conductivity and diffusivity values for the probe and the sediment, as well as the initial friction-induced temperature rise and the final equilibrium temperature. The modeling process takes the first minute of the cooling data, and then uses the resulted parameter values in the FE simulation to predict the temperature for the rest of recording. The differences between the predicted and observed values beyond the 1-min recording time yield an extrapolation misfit RMS for each sensor probe.

[41] We use several quantitative criteria to screen the models. First, the model misfit RMS must be less than

0.002 C and the extrapolation misfit RMS is less than 0.004 C. Second, the ratio of the GA-IM derived thermal conductivity value to the value obtained for an instantaneous line source (of which the heat release was computed from the model initial temperature rise and the probe's model heat capacity) should stay within 5% from unity. Third, the GA-IM equilibrium temperature should be within 0.002 C of the value obtained independently from the conventional extrapolation to time infinite through the relation of temperature-versus-inverse time. The first model RMS criterion is typical for inverse modeling. We add randomness to the initial input parameter values through GA and use extrapolation misfit to gauge how well a GA-IM model can predict the cooling behavior that plays no role in parameter determination per se. The third criterion accepts the conventional premise that asymptotically, the temperature declines in proportion to inverse time for an instantaneously heated line source. The second criterion provides a consistency test among the "independent" model parameters: The total heat release needed to estimate thermal conductivity via the asymptotic relation is computed from the initial temperature rise and a sensor probe's heat capacity, both of which are output of the GA-IM modeling. Thus our method incorporates both GA-IM and a well-established practice for marine heat flow measurement.

[42] We run the stochastic GA-IM process at least 10 times, each of which uses hundreds or thousands combinations of parameter values within wide ranges of possible values, to generate 10 models that meet the three selection criteria. The mean value of the desired parameter values for those 10 acceptable models is deemed as the final representative value. The standard deviation from the mean is regarded as the uncertainty for that particular parameter (e.g., equilibrium temperature, and thermal conductivity and diffusivity). The average relative difference between the temperatures determined from conventional method and Lee's method is 3.06% with a standard deviation of 0.38%.

B2. Heat Flux

[43] A steady heat flux q through a medium of varying thermal conductivity but free of internal heat generation and any mass movement is, according to Fourier's law in one dimension,

$$q = (T - T_{ref})/\int_{z_{ref}}^{z} \frac{dz}{k} \qquad (B1)$$

where T_{ref} is the temperature at the reference depth z_{ref} with q being upward positive and z being downward positive. Because k is given only at eight discrete points where the probes are located, there are several ways to integrate equation (B1) numerically. The simplest is to assume a constant conductivity over one depth interval. For example, a set of seven interval heat fluxes can be estimated from

$$q_i = \overline{k_i} \frac{T_{i+1} - T_i}{z_{i+1} - z_i} \qquad (B2)$$

where $i = 1$ to $M - 1$ ($M = 8$ is the number of probes). The interval conductivity $\overline{k_i}$ is approximated by the harmonic mean of k_i and k_{i+1}. The mean of the seven interval heat fluxes is taken as the heat flux at the site or station.

[44] An alternative way to determine heat flux is first to find a quadratic interpolation relation:

$$k = \alpha + \beta z + \gamma z^2, z_{j-1} \leq z \leq z_{j+1} \qquad (B3)$$

for k_{j-1}, k_j, and k_{j+1} (j = 2, 3, .., 7), where α, β, and γ are regression constants. Then, substitute this relation into equation (B1) to yield an interval heat flux over the depth interval from z_{j-1} to z_{j+1}. There are six so defined interval heat fluxes. In this way, each depth interval (except the top and bottom ones) is assigned with two depth-overlapping values; the mean of the two values is taken as the interval heat flux. After correcting for overlapping, there are seven interval heat fluxes. The mean of those seven interval values is taken as the heat flux at the site. The two methods yield a difference of about 1 to 2%. This second approach is used here to calculate the heat fluxes.

References

Anderson, R. N., M. G. Langseth, and J. G. Scalter (1977), The mechanisms of heat transfer through the floor of the Indian Ocean, *J. Geophys. Res.*, 82, 3391–3409.

Anderson, R. N., M. A. Hobart, and M. G. Langseth (1979), Geothermal convection through oceanic crust and sediments in the Indian Ocean, *Science*, 204, 828–832.

Becker, K., and E. E. Davis (2004), In situ determinations of the permeability of the oceanic igneous crust, in *Hydrogeology of the Oceanic Lithosphere*, edited by E. E. Davis and H. Elderfield, pp. 189–224, Cambridge Univ. Press, New York.

Belkin, I. M., and A. L. Gordon (1996), Southern Ocean fronts from the Greenwich meridian to Tasmania, *J. Geophys. Res.*, 101, 3675–3696.

Ben Zion, Y., Z. Peng, D. Okaya, L. Seeber, J. G. Armbruster, N. Ozer, A. J. Michael, S. Baris, and M. Aktar (2003), A shallow fault-zone structure illuminated by trapped waves in the Karadere-Duzce branch of the North Anatolian Fault, western Turkey, *Geophys. J. Int.*, 152, 699–717.

Bryant, W. R., A. P. Deflache, and P. K. Trabant (1974), Consolidation of marine clays and carbonates, in *Deep Sea Sediments: Physical and Mechanical Properties*, edited by A. L. Inderbitzen, pp. 209–244, Plenum, New York.

Bullard, E. C. (1954), The flow of heat through the floor of the Atlantic Ocean, *Proc. R. Soc. London, Ser. A*, 222, 408–429.

Carbotte, S. M., et al. (2004), New integrated data management system for Ridge2000 and MARGINS research, *Eos Trans. AGU*, 85(51), 553.

Christie, D. M., D. G. Pyle, R. B. Pedersen, and D. J. Miller (2004), Leg 187 synthesis: Evolution of the Australian Antarctic Discordance, the Australian Antarctic depth anomaly, and the Indian/Pacific mantle isotopic boundary, *Proc. Ocean Drill. Program Sci. Results*, 187, 1–41. (Available at http://www-odp.tamu.edu/)

Davis, E. E., and H. Elderfield (2004), *Hydrogeology of the Ocean Crust*, 706 pp., Cambridge Univ. Press, New York.

Davis, E. E., and C. R. B. Lister (1974), Fundamentals of ridge crest topography, *Earth Planet. Sci. Lett.*, 21, 405–413.

Davis, E. E., K. Wang, J. He, D. S. Chapman, H. Villinger, and A. Rosenberger (1997), An unequivocal case for high Nusselt number hydrothermal convection in sediment buried igneous oceanic crust, *Earth Planet. Sci. Let.*, 146, 137–150.

Davis, E. E., D. S. Chapman, K. Wang, H. Villinger, A. T. Fisher, S. W. Robinson, J. Grigel, D. Pribnow, J. Stein, and K. Becker (1999), Regional heat flow variations across the sedimented Juan de Fuca Ridge eastern flank: Constraints on lithospheric cooling and lateral hydrothermal heat transport, *J. Geophys. Res.*, 104, 17,675–17,688.

Davis, E. E., K. Wang, K. Becker, R. E. Thomson, and I. Yashayaev (2003), Deep-ocean temperature variations and implications for errors in seafloor heat flow determinations, *J. Geophys. Res.*, 108(B1), 2034, doi:10.1029/2001JB001695.

Dezileau, L., G. Bareille, J.-L. Reyss, and F. Lemoine (2000), Evidence for strong sediment redistribution by bottom currents along the Southeast Indian Ridge, *Deep Sea Res.*, 47, 1899–1936.

Engdahl, E. R., R. D. Van der Hilst, and R. P. Buland (1998), Global teleseismic earthquake relocation with improved travel times and procedures for depth determination, *Bull. Seismol. Soc. Am.*, 88, 722–743.

Fisher, A. T., and K. Becker (1995), Correlation between seafloor heat flow and basement relief: Observational and numerical examples and implications for upper crustal permeability, *J. Geophys. Res.*, 100, 12,641–12,657.

Fisher, A. T., and K. Becker (2000), Channelized fluid flow reconciles heat-flow and permeability data, *Nature*, 403, 71–74.

Goodell, H. G., R. Houtz, M. Ewing, D. Hayes, B. Naini, R. J. Echols, J. P. Kennett, and J. G. Donahue (1973), Marine sediments of the southern oceans, *Antarct. Map Folio Ser.*, Folio 17, Am. Geogr. Soc., New York.

Hayes, D. E. (1991), *Marine Geological and Geophysical Atlas of the Circum-Pacific to 30°S*, *Antarct. Res. Ser.*, vol. 54, AGU, Washington, D. C.

Hyndmann, R. D., A. J. Erickson, and R. P. Von Herzen (1974), Geothermal measurements on DSDP Leg 26, *Initial Rep. Deep Sea Drill. Proj.*, 26, 451–463.

Jacobs, S. S., E. Bauer, P. M. Bruchhausen, A. L. Gordon, R. M. Root, and F. Rosselot (1974), Eltanin reports: Cruises 47–50; 52–55, *Tech. Rep. CU-2–74*, Lamont-Doherty Geol. Obs., Columbia Univ., Palisades, N. Y.

Jemsek, J., and R. P. Von Herzen (1989), Measurement of in situ sediment thermal conductivity: Continuous heating method with outrigged probes, in *Handbook of Seafloor Heat Flow*, edited by J. A. Wright and K. E. Louden, pp. 91–120, CRC Press, Boca Raton, Fla.

Kunze, E., and S. Llewellyn Smith (2004), The role of small scale topography in turbulent mixing of the global ocean, *Oceanography*, 17, 55–64.

Labails, C. (2001), Etude qualitative et quantitative des données de flux de chaleur de la campagne ANTAUS, memoire de Maıcirc;trise, Univ. de Bretagne Occidentale, Brest, France.

Langseth, M. A., and P. I. Taylor (1967), Recent measurements in the Indian Ocean, *J. Geophys. Res.*, 72, 6249–6260.

Langseth, M. G. (1965), Techniques of measuring heat flow through the ocean floor, in *Terrestrial Heat Flow*, *Geophys. Monogr. Ser.*, vol. 8, edited by W. H. K. Lee, pp. 58–77, AGU, Washington, D. C.

Langseth, M. G., and B. M. Herman (1981), Heat transfer in the oceanic crust of the Brazil Basin, *J. Geophys. Res.*, 86, 10,805–10,819.

Lee, T. C., and R. P. Von Herzen (1994), In situ determination of thermal properties of sediments using a friction-heated probe source, *J. Geophys. Res.*, 99, 12,121–12,132.

Lee, T. C., A. D. Duchkov, and S. G. Morozov (2003), Determination of thermal conductivity and formation temperature from cooling history of friction-heated probes, *Geophys. J. Int.*, 152, 433–442.

Lister, C. R. B. (1972), On the thermal balance of a mid-oceanic ridge, *Geophys. J. R. Astron. Soc.*, 26, 515–535.

Lister, C. R. B. (1977), Estimators for heat flow and deep rock properties based on boundary layer theory, *Tectonophysics*, 41, 157–171.

Lockner, D., H. Naka, H. Tanaka, H. Ito, and R. Ikeda (2000), Permeabilities and strength of core samples for the Nojima fault of the 1995 Kobe Earthquake, *U.S. Geol. Surv. Open File Rep.*, OF 00-0129, 147–152.

Louden, K. E., and J. A. Wright (1989), Marine heat flow: A new compilation of observations and brief review of its analysis, in *Handbook of Seafloor Heat Flow*, edited by J. A. Wright and K. E. Louden, pp. 3–70, CRC Press, Boca Raton, Fla.

Mantyla, A. W., and J. Reid (1995), On the origins of deep and bottom waters of the Indian Ocean, *J. Geophys. Res.*, 100, 2417–2439.

Marks, K., J. Stock, and K. Quinn (1999), Evolution of the Australian Antarctic Discordance since Miocene time, *J. Geophys. Res.*, 104, 4967–4981.

Mauritzen, C., K. L. Polzin, M. S. McCartney, R. C. Millard, and D. E. West-Mack (2002), Evidence in hydrography and density fine structure for enhanced vertical mixing over the Mid-Atlantic Ridge in the western Atlantic, *J. Geophys. Res.*, 107(C10), 3147, doi:10.1029/2001JC001114.

Petterson, H. (1949), Exploring the bed of the ocean, *Nature*, 164, 468–470.

Pribnow, D. F. C., M. Kinoshita, and C. A. Stein (2000), Thermal data collection and heat flow recalculations for ODP legs 101–180, *Rep. 0120432*, Inst. for Jt. Geosci. Res., Leibniz Inst. for Appl. Geosci.,

Hannover, Germany. (Available at http://www-odp.tamu.edu/publications/heatflow/)

Rodman, M. R., and A. L. Gordon (1982), Southern Ocean bottom water of the Australian-New Zealand sector, *J. Geophys. Res.*, *87*, 5771–5778.

Royer, J.-Y., and D. T. Sandwell (1989), Evolution of the eastern Indian Ocean since the Late Cretaceous: Constraints from Geosat altimetry, *J. Geophys. Res.*, *94*, 13,755–13,782.

Sclater, J. G. (2004), Variability of heat flux through the sea-floor: Discovery of hydrothermal circulation in the ocean crust, in *Hydrogeology of the Oceanic Lithosphere*, edited by E. E. Davis and H. Elderfield, pp. 3–27, Cambridge Univ. Press, New York.

Sclater, J. G., J. Crowe, and R. N. Anderson (1976), On the reliability of oceanic heat flow averages, *J. Geophys. Res.*, *81*, 2997–3006.

Smith, W. H. F., and D. T. Sandwell (1994), Bathymetric prediction from dense satellite altimetry and sparse shipboard bathymetry, *J. Geophys. Res.*, *99*, 21,803–21,824.

Somerville, M., D. Wyborn, P. N. Chopra, S. S. Rahman, D. Estrella, and T. Van der Meulen (1994), Hot dry rocks feasibility study, *Rep. 94/243*, 133 pp., Aust. Energy Res. and Dev. Corp., Canberra.

Stein, C. A., and S. Stein (1992), A model for the global variation in oceanic depth and heat flow model with lithospheric age, *Nature*, *359*, 123–128.

Stein, C. A., and S. Stein (1994), Constraints on hydrothermal heat flux through the oceanic lithosphere from global heat flow, *J. Geophys. Res.*, *99*, 3081–3095.

Von Herzen, R. P. (2004), Geothermal evidence for continuing hydrothermal circulation in older (>60 Ma) ocean crust, in *Hydrogeology of the Oceanic Lithosphere*, edited by E. E. Davis and H. Elderfield, pp. 414–447, Cambridge University Press.

Von Herzen, R. P., and M. G. Langseth (1966), Present status of oceanic heat-flow measurements, *Phys. Chem. Earth*, *6*, 365–407.

Von Herzen, R. P., and A. E. Maxwell (1959), The measurement of thermal conductivity of deep sea sediments by a needle probe method, *J. Geophys. Res.*, *64*, 1557–1563.

Weissel, J. K., and D. E. Hayes (1974), The Australian-Antarctic Discordance: New results and implications, *J. Geophys. Res.*, *79*, 2579–2587.

Wessel, P., and W. H. F. Smith (1991), Free software helps map and display data, *Eos Trans. AGU*, *72*, 441.

————————————

D. Abbott and J. R. Cochran, Lamont Doherty Geological Observatory of Columbia University, 109 Oceanography, Palisades, NY 10964, USA.

D. Appriou, L. Géli, and C. Labails, Marine Geosciences Department, Ifremer, BP 70, Plouzané F-29280, France. (louis.geli@ifremer.fr)

J. Francheteau, Institut Universitaire Européen de la Mer, Place Nicolas Copernic, Plouzané F-29280, France.

T. C. Lee, Department of Earth Sciences, University of California, Riverside, Riverside, CA 92521, USA.